Nanoscale

Accepted Manuscript

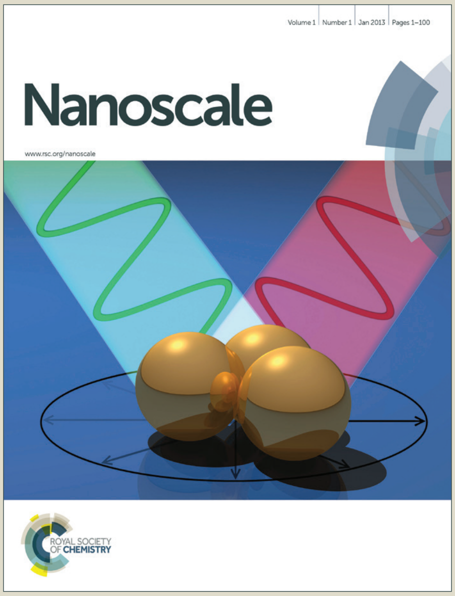

ROYAL SOCIETY OF CHEMISTRY

www.rsc.org/nanoscale

Nanoscale RSCPublishing

REVIEW ARTICLE

Cite this: DOI: 10.1039/x0xx00000x

Nanoparticle Conversion Chemistry: Kirkendall Effect, Galvanic Exchange, and Anion Exchange

Bryan D. Anderson and Joseph B. Tracy*

Received 00th January 2012,
Accepted 00th January 2012

DOI: 10.1039/x0xx00000x

www.rsc.org/

Conversion chemistry is a rapidly maturing field, where chemical conversion of template nanoparticles (NPs) into new compositions is often accompanied by morphological changes, such as void formation. The principles and examples of three major classes of conversion chemical reactions are reviewed: reactions of metal NPs exhibiting the Kirkendall effect, galvanic exchange, and anion exchange, each of which can result in void formation in NPs. These reactions can be used to obtain complex structures that may not be attainable by other methods. During each kind of conversion chemical reaction, NPs undergo distinct chemical and morphological changes, and insights into the mechanisms of these reactions will allow for improved fine control and prediction of the structures of intermediates and products. Conversion of metal NPs into oxides, phosphides, sulphides, and selenides often occurs through the Kirkendall effect, where outward diffusion of metal atoms from the core is faster than inward diffusion of reactive species, resulting in void formation. In galvanic exchange reactions, metal NPs react with noble metal salts, where a redox reaction favours reduction and deposition of the noble metal (alloying) and oxidation and dissolution of the template metal (dealloying). In anion exchange reactions, addition of certain kinds of anions to solutions containing metal compound NPs drives anion exchange, which often results in significant morphological changes due to the large size of anions compared to cations. Conversion chemistry thus allows for the formation of NPs with complex compositions and structures, for which numerous applications are anticipated arising from their novel catalytic, electronic, optical, magnetic, and electrochemical properties.

1. Introduction

Conversion chemistry is a versatile approach for the templated chemical conversion of nanoparticles (NPs) of one composition into another, which is often accompanied by morphological changes or nanostructural transformations, such as void formation.[1–3] A common set of reaction mechanisms governing NP conversion chemistry is reviewed here. Introducing reactive species to preformed NPs drives morphological changes that are determined by the interaction between chemical reactions and diffusion of atomic species or charge carriers throughout the NP.[4] Many conversion chemical reactions occur autocatalytically, where the reaction occurs at one or a small number of reaction sites in the NP. The number and distribution of these reaction sites is important for determining the nanostructural evolution.

This review is focused chiefly on understanding and controlling conversion chemical reactions and the accompanying morphological changes in NPs. As the field matures, emphasis will increasingly shift from understanding conversion chemistry toward controlling it and optimizing it for applications. Recent advances in NP conversion chemistry are summarized, where individual NPs undergo significant morphological changes. The particular classes of conversion chemical reactions discussed in this review include the Kirkendall effect during reactions of metal NPs, galvanic exchange, and anion exchange, which is often accompanied by the Kirkendall effect (Scheme 1). A common type of conversion chemical reaction is alloying or compounding of atomic species through a diffusion couple, which often results in porous structures (Scheme 1a).[5–8] Void formation can occur within NPs when species from the NP core diffuse outward more quickly than inward diffusion of reactive species, causing the reaction to occur on or near the NP surface. Void formation as a result of the imbalance of diffusion rates is a manifestation of the Kirkendall effect. While void formation is well known in metallurgy as leading to mechanical failure at interfaces between materials, void formation on the nanoscale can be well controlled due to geometrical confinement of diffusion.[9–12] The Kirkendall effect in nanostructures has garnered significant attention because of its frequent occurrence and the possibility to obtain uniquely tailored structures with well controlled compositions and structures.[13] Our review of the Kirkendall

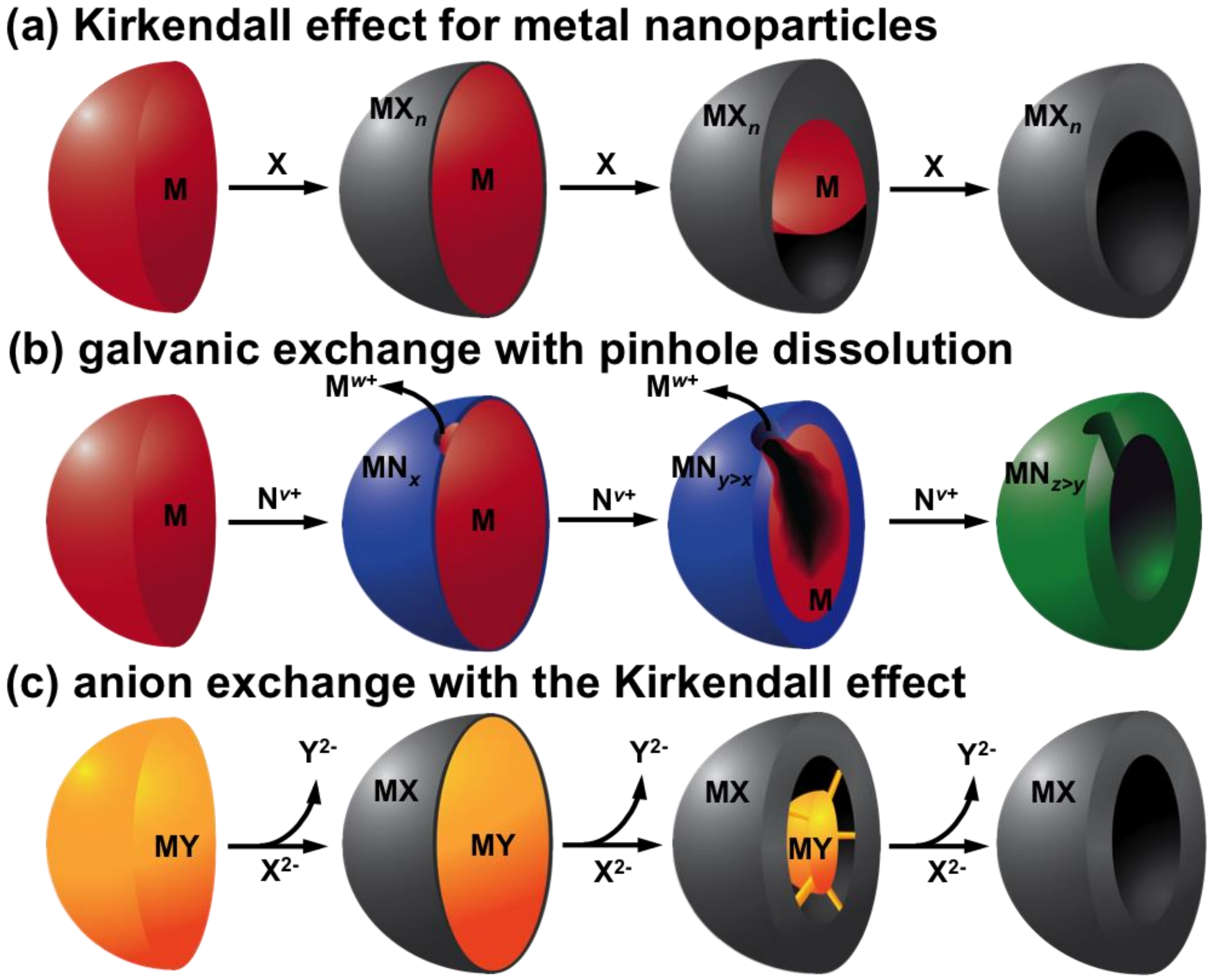

Scheme 1. Graphical depictions of examples of conversion chemical reactions of NPs. (a) Kirkendall effect: During the reaction of the metal (M) with reactive species X to form MX_n, void formation occurs. (b) Galvanic exchange: Reduction of ions (N^{v+}) of a more noble metal (N) drives oxidation of a less noble metal (M), which dissolves into solution (M^{w+}) through pinholes formed in the shell. (c) Anion exchange: During the reaction of a metal compound (MY) with a reactive anion (X^{2-}), anions (Y^{2-}) are released to form MX. Void formation through the Kirkendall effect can occur when cations diffuse outward to react with the reactive anions.

effect in metal NPs is focused on how to obtain compositional and morphological control during reactions of metal NPs.

Chemical transformation of NPs via galvanic exchange (also known as transmetalation) is another versatile and promising method for creating designer NPs with tailored morphologies, thereby altering their physical properties (Scheme 1b).[14–17] Galvanic exchange is driven by the difference in reduction potentials between two metals.[18] After synthesizing a nanostructure of the less noble metal, a solution containing cations of a more noble element (lower reduction potential) is added. The less noble metal NP serves as a sacrificial template, from which some portion of the metal is oxidized and transferred back into solution concurrently with reduction and deposition of the more noble metal. Au, Pt, and Pd salts have often been chosen as the more noble metals.[19] During galvanic exchange reactions, the structure and composition of the products are further affected by the interaction between the more and less noble metals. Initially, alloy shells usually grow on the less noble metal NP.[20] As galvanic exchange proceeds, dealloying may also occur, where the less noble metal is removed from the alloy. Alloying and dealloying drive morphological changes (often into hollow nanostructures, which sometimes appear as nanoframes). The final stage of dealloying often leads to breakup of the nanostructure, which is often avoided by stopping galvanic exchange reactions before completion.

Anion exchange is an ion exchange reaction, where anions in the template NPs are extracted and replaced through addition of another kind of anion. Cation exchange is a more common kind of ion exchange reaction, where the cations are replaced. The smaller ionic radius of cations than anions facilitates diffusion while conserving the morphology of the template NP.[21,22] Partial cation and partial anion exchange can promote the fabrication of heterostructured or hybrid NPs with tailored structures and properties.[23,24] Cation exchange has recently been extensively reviewed elsewhere and is not further discussed here. We refer the interested reader to these other review articles.[25,26]

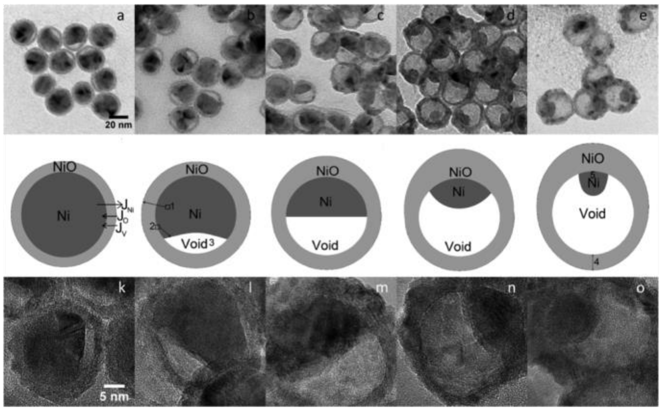

Fig. 1 TEM and corresponding graphical depictions of the morphological evolution through the Kirkendall effect during the oxidation of 26 nm diameter Ni NPs under ambient atmosphere at 300 °C for (a,k) 90, (b,l) 120, (c,m) 150, (d,n) 180, and (e,o) 210 min. Formation of a single void at the core/shell interface causes asymmetrical outward diffusion of Ni, resulting in a non-uniform NiO shell thickness. Reprinted with permission from Reference 43. © 2010 American Chemical Society.

The size and morphology of NPs can be controlled through several mechanisms, including Ostwald ripening.[27–30] While Ostwald ripening is not accompanied by a conversion chemical reaction (and thus is not covered here is significant detail), it can have an important role in the coalescence of voids, shape changes, and phase transformations in nanostructures.[31,32] A recent review discusses advances in the synthesis of SnO_2, TiO_2, Fe_2O_3, Co_3O_4, and complex metal oxide hollow NPs through Ostwald ripening.[2]

2. Mechanisms and Examples of Nanoparticle Oxidation

A. Introduction to Oxidation

Oxidation is a common NP conversion chemical reaction.[33–36] Oxidation of NPs involves a process similar to oxidation of bulk metals, where a thin oxide layer forms on the metal surface, followed by simultaneous outward diffusion of metal ions through the oxide scale and inward diffusion of oxygen into the NP.[5,37,38] Metal ions often diffuse more quickly outward than oxygen diffuses inward, which is consistent with the larger ionic radius of anions than cations. The balance of diffusion rates determines the structure of the oxidized product. More complex structures, rather than simply incorporating oxygen in the initial structure wherever the metal is present, can emerge when outward diffusion of the metal is significant.[39] Several theories used to describe the initial stages of oxidation of bulk metals can also be applied to explain nanostructural changes in NPs that accompany oxidation.[40–42] The oxidation conditions and template NP composition, size, and shape give rise to different regimes of oxidation behaviour and determine the composition and structure of intermediates and the final product, such as whether voids form and how they are arranged.[43]

If inward diffusion of oxidizing species into NPs is faster than outward diffusion of metal cations, then the NP shape (neglecting a change in volume to accommodate oxygen incorporation) is typically preserved. Such behaviour is often observed at the initial stages of oxidation. At intermediate stages of oxidation, core/shell structures are often observed, for which several examples are known.[7,13,33,34,36,43–69] The Kirkendall effect, where outward diffusion of the metal is faster than inward diffusion of oxygen, can drive substantial morphological changes during NP oxidation (Fig. 1).

B. Cabrera-Mott (CM) Theory of Oxidation and Formation of Thin Oxide Films

Cabrera-Mott (CM) theory is one of the first physical rather than phenomenological models to describe diffusion of metal ions and oxygen during oxidation.[70] CM theory was initially developed to model oxidation of a flat slab of material rather than a curved NP but nevertheless provides a good description of the onset of metal NP oxidation. More recent modifications to CM theory take into account spherical NP geometries along with core and shell volume changes during oxidation.[71,72] Auge *et al*. have also included a parameter for the influence of surface-bound stabilizing ligands for modelling oxidation of colloidal NPs.[73]

CM theory describes the first stage of oxidation, where oxygen initially disassociates and adsorbs onto the surface of the metal, forming a thin metal oxide layer. Adsorption of oxygen creates surface states below the Fermi energy of the metal.[74] Electron tunnelling into the surface states results in an electric field within the oxide that lowers the activation energy for diffusion of metal cations, which then commences.[71] The electric field is critical for driving migration of metal cations, which is initially fast because the electric field depends inversely on the oxide layer thickness (Scheme 2). As the oxide layer grows thicker, the electric field decreases, which reduces the rate of migration and slows further oxidation. The self-limiting nature of the CM mechanism of oxidation results in very slow oxidation of thicker films, and other oxidation mechanisms become predominant, provided the temperature is sufficiently high. In CM theory, electron tunnelling is rapid, and diffusion of metal cations from the metal/oxide interface to the oxide/solution or oxide/gas interface is assumed to be rate determining. CM theory without any further modifications is only valid for thin oxide layers (< 3 nm) and relies upon several assumptions that limit its scope. For example, CM theory does not take grain boundaries into account and assumes the defect concentration remains constant throughout the entire oxidation process. More recent modifications to CM theory overcome these limitations, but the original CM theory remains useful for explaining and predicting the initial stage of NP oxidation.

C. Comparison of Cabrera-Mott Theory with Experiment

CM theory has been used extensively to explain low-temperature oxidation kinetics of metal NPs. Yoon *et al*.[36] investigated oxidation of elemental Fe NPs. Oxide shells formed nonlinearly with time in air at room temperature. Understanding and controlling NP oxidation kinetics is important because physical properties (magnetic properties, in this example) depend on both the structure and composition of the iron oxide formed.[49,75] As expected, the magnetization decreased as the oxide thickness increased. Oxidation kinetics did not depend on the NP size; rather, oxide shells formed on different NP sizes with the same initial thickness of 2.2 nm (Fig. 2).[36] In another study, also under ambient conditions, growth of iron oxide shells on Fe NPs of different sizes exhibited the same time dependence.[49] Therefore, the mechanism of initial oxidation does not depend on size. NPs with diameters below 8 nm were completely oxidized and usually contained a single void in the centre. Sizes larger than 10 nm, however, formed core/shell NPs containing an α-Fe core with a shell consisting of either Fe_3O_4 or γ-Fe_2O_3. In the core/shell NPs, multiple voids formed at the core/shell

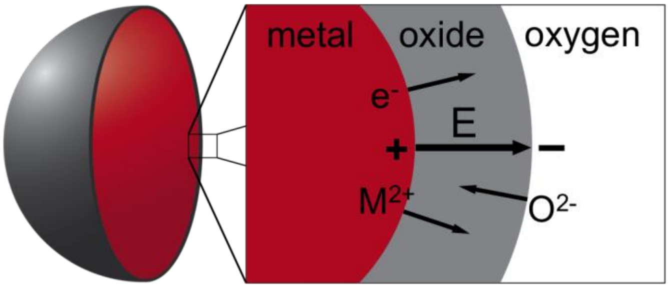

Scheme 2. Graphical depiction of the initial stages of oxidation of a metal NP according to the Cabrera-Mott model, resulting in a thin metal oxide layer. An electric field generated in the metal oxide layer drives diffusion of ions and flow of electrons through the oxide layer. Inward diffusion of O_2^- is predominant for thin oxide layers.

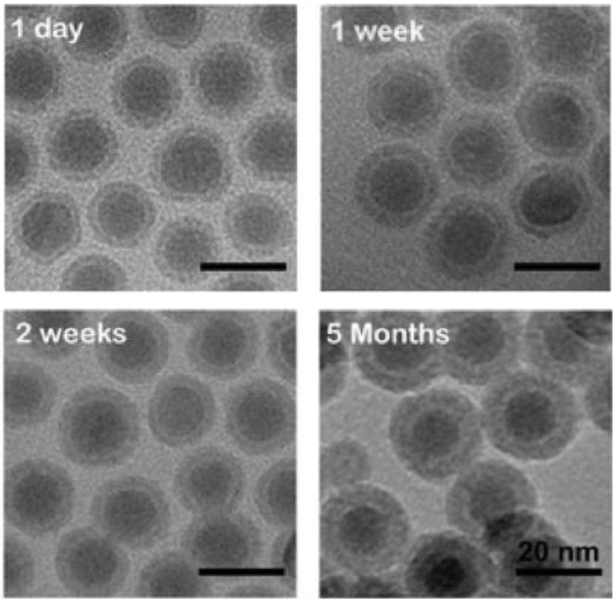

Fig. 2 TEM images showing the formation of thin oxide shells on Fe NPs in air at room temperature. After rapid formation of the initial thin oxide, the oxidation rate slows by several orders of magnitude. Reprinted with permission from Reference 36. © 2013 WILEY-VCH Verlag GmbH & Co. KGaA, Weinheim.

interface. While the oxide formation rate in Fe NPs substantially slows as the oxide shell thickness increases, the rate and extent of NP oxidation can be increased by raising the temperature.[7] Oxidation of metals is thermodynamically favourable but kinetically hindered. It should be noted that $\Delta S°$ < 0 for oxidation, since gaseous oxygen is consumed and is the most significant contribution to entropy. Consequently, raising the temperature makes $\Delta G°$ for oxidation more positive.

Size-independent oxidation of Co NPs has also been confirmed.[76] Co NPs with diameters below 5 nm were immediately completely oxidized and reshaped into hollow shells through the Kirkendall effect. Moreover, oxidation of Co NPs under ambient atmosphere and temperature exhibits a logarithmic dependence on time, as predicted by CM theory.[76]

Colloidal NPs are typically stabilized in solution by organic ligands, which can inhibit oxidation and alter the oxidation kinetics and the structure of the oxide products. Doan *et al.*[76] compared the oxidation of Co NPs stabilized by amines and carboxylic acids by measuring the oxygen consumption. For tridodecylamine-stabilized Co NPs, an oxide thickness of 0.8 nm was obtained after 3000 s of oxidation. The tridodecylamine groups were then replaced with carboxylic acids of varying chain lengths via ligand exchange. The oxide shell thickness on the carboxylic acid-stabilized NPs after 3000 s of oxidation was 1.2 nm. After 6 months of exposure to atmospheric oxygen, tridodecylamine- and carboxylic acid-stabilized Co NPs formed Co/CoO core/shell and hollow CoO NPs, respectively. Promotion of oxidation by carboxylic acid ligands was attributed to carboxylate anions formed on the NP surface, which enhanced the electric field associated with oxidation through the CM mechanism and allowed for a greater flux of Co(II). The functional group appears to have a more pronounced effect than steric effects that could restrict O_2 from reaching the NP surface, since a bulky tertiary amine would less effectively block access to the core than an unbranched carboxylic acid. It should also be noted that the electron beam of a TEM can drive oxidation of Co NPs into CoO, where carboxylic acid ligands are believed to serve as the source for O^{2-}. Such electron-beam driven oxidation also alters the subsequent oxidation behaviour under ambient atmosphere.[34]

NP oxidation can be problematic for air-sensitive NP core materials, where there is interest in controlling the extent of oxidation or completely avoiding it. Self-assembly of ligand-stabilized Ag and Co NPs into close-packed monolayers has been shown to inhibit oxidation.[77–80] Yang *et al.* investigated the oxidation of Co NPs supported on TEM grids, where they compared dilute dispersions with close-packed assemblies. Dilute dispersions of Co NPs completely oxidized into CoO NPs, but close-packed arrays partially oxidized into Co/CoO core/shell NPs.[81] Another study demonstrated control over void formation by creating metal core / alloy shell Fe/Fe$_x$Cr$_{1-x}$ NPs.[82] Upon oxidation, the NPs were transformed into Fe/M_3O_4 (M = Fe, Cr) core/shell NPs. Depending on the initial Fe$_x$Cr$_{1-x}$ alloy shell thickness, the Kirkendall effect was minimized or prevented. NPs with thin alloy shells, however, still formed voids.

A study by Nakamura *et al.*[83] on the low-temperature oxidation of Cu, Al, and Pb NPs provided insights into the mechanisms of NP oxidation. For some compositions, a critical NP diameter for complete oxidation at or near room temperature was observed. For NPs smaller than the critical diameter, a single void was formed through the Kirkendall effect in the completely oxidized product. For NPs larger than the critical diameter, oxidation was incomplete, and some of the reduced metal remained in the core, while voids formed between the core and shell. Al NPs had a critical diameter of < 8 nm, and the Al_2O_3 shell thickness was 1.5 nm. In another study by Nakamura *et al.*, Zn NPs exhibited a critical diameter of < 20 nm for hollow NP formation.[53] The critical diameter for Cu NPs is in the range of 10-40 nm.[53] The Kirkendall effect was not observed for the oxidation of Pb NPs, but oxidation to PbO was complete. They concluded that CM theory applies to the low-temperature oxidation of Cu, Al, and Pb NPs, while different mechanisms determine the extent of void formation during oxidation in each of type of NP.[83] The lower critical diameter for void formation for Cu than Al can be explained by the much higher self-diffusion coefficient of Cu than Al and the much lower vacancy formation energy for Cu than for Al. While the initial oxidation of Cu and Al is consistent with CM theory, the slower self-diffusion of Al causes Al NPs to more clearly demonstrate the limiting behaviour of CM theory, when the electric field is diminished as the oxide shell grows. Beyond initial oxidation and at sufficiently high temperatures, oxidation proceeds according to other diffusion mechanisms.

D. Theories for High-Temperature Oxidation through Lattice Diffusion – from Bulk Metals to Nanoparticles

While oxidation reactions are common, the mechanisms of NP oxidation remain incompletely understood. Tunnelling and the electric field described by CM theory are only viable for thin oxide layers. Other oxidation mechanisms must be considered to properly describe the further and complete oxidation of metal NPs. Jia *et al*. found that the room-temperature oxidation kinetics of Co NPs proceeded according to a logarithmic rate expression at thicknesses, where CM theory would no longer apply.[84] While the initial stage of oxidation described by CM theory has been quantitatively compared with experiment, most comparisons for subsequent oxidation with experiment are phenomenological rather than quantitative.

Wagner theory[85] was originally developed to describe high-temperature oxidation of bulk metals beyond the thin layers described by CM theory. During oxide scale growth, Wagner theory assumes the oxide scale is dense, continuous, and conformal with the underlying metal surface. Thermodynamic equilibrium throughout the oxide layer and at the metal/oxide and oxide/oxygen interfaces is also assumed. Lattice diffusion of ions and charges across the neutral oxide layer is presumed to be the rate-limiting step, which gives a parabolic rate expression for oxide growth.[86,87]

NP oxidation is more accurately described by several other theories and additional modifications to CM theory. Valensi-Carter's shrinking core model for isothermal high-temperature oxidation of spherical particles takes into account the spherical geometry, resulting in a more accurate rate law for oxidation.[88–91] Fromhold and Cook have modified CM theory to arrive at a more general theory of planar thick oxide film growth using a coupled-current approach that accounts for diffusion of ions and charge carriers in the presence of large surface charges and large space charges within the oxide layer. The growth kinetics of metal oxide films can be modeled by accounting for all of the ionic and electronic diffusion currents.[92] CM theory's single-current model represents the low space-charge, high electric-field limit of Fromhold and Cook's theory. Twenty years later, Fromhold developed a model for the oxidation of spherical metal NPs in the low space-charge limit using the coupled current approach for oxide thicknesses below 100 nm.[93] In contrast, CM theory describes formation of thin (< 10 nm), planar metal oxide layers. Since NP reaction rates and activation energies depend on size and shape, Fromhold's model of nanoscale oxide formation is more accurate but also more complex than CM theory. An experimental study used Fromhold's theory and Valensi-Carter's shrinking core model to understand oxidation kinetics of Ni NPs; the activation energy for NP oxidation decreases with size.[94] More recently, other modifications of CM theory for spherical NPs have been developed.[71–73,95]

E. Void Instability: Reductive Transformations and High-Temperature Collapse

Conducting successive conversion chemical reactions on NPs can be envisioned to create complex structures. Pairing oxidation with reduction by vacuum, H_2, or other reducing atmospheres[62,65,66,96] allows investigations of the "reversibility" of the oxidation process with respect to the intermediate and final structures, as well as the conversion mechanism. Moreover, if sintering between NPs can be avoided during oxidation and reduction, then cyclic oxidation-reduction reactions can be performed.

Ha *et al*.[97] demonstrated a cyclic chemical and morphological transformation between Mn_3O_4/SiO_2 core/shell NPs with small metal oxide (PtO, PdO, NiO) NPs embedded in the SiO_2 shell and hollow $MnO-SiO_2$ NPs with small embedded metal NPs (Pt, Pd, Ni), which is obtained by heating under H_2 (Fig. 3). Mn(III) is reduced to Mn(II) and diffuses into the SiO_2 shell. Further oxidation in air at elevated temperature converted the NPs back into their former structure, and the NPs were reversibly cycled between the two structures by toggling between reducing and oxidizing conditions. The use of SiO_2 shells was effective at preventing sintering among the NPs, provided that excessively high temperatures were not used.

Medford *et al*.[66] investigated the size-dependent reduction of hollow/porous NiO NPs of several sizes with H_2 at 500 °C that had been obtained from solid Ni NPs through the Kirkendall effect. The nanostructures and distribution of Ni and NiO before, during, and after reduction depend on the size of the template NPs. Small hollow NiO NPs (obtained from solid Ni NPs with diameters of 12 nm) were found to have a single Ni nucleation site inside the hollow cavity at the void/NiO interface. As reduction proceeded, Ni was deposited inside the void. The NiO shells are expected to have some porosity, which would allow H_2 to diffuse through the shells. Chenna *et al*. investigated the reduction of NiO nanoshells supported on larger SiO_2 NPs and similarly observed the growth of single Ni grains that nucleated on the inside of the NiO nanoshells at the NiO/SiO_2 interface.[62,65] Medford *et al*. also studied the reduction of larger NiO NPs, for which multiple Ni grains nucleated and served as reduction sites.[66] For example, during the reduction of hollow NiO NPs formed from Ni NPs initially of diameter 24 nm, multiple Ni grains formed within the NiO shell rather than on its surface, which is a type of structure that was not obtained during the initial oxidation procedure. As reduction progressed in the larger NPs, Ni grains grew, and then Ni/NiO NPs eventually collapsed.

Sadasivan *et al*.[68] investigated the cyclic reduction-oxidation-reduction of cube-shaped Co_3O_4 NPs with sizes of 3, 6, 11, and 29 nm. During the first reduction reaction with H_2 at 500 °C, conversion into spherical Co NPs occurred. Upon subsequent oxidation, the 3 and 6 nm samples were completely oxidized into solid CoO and/or Co_3O_4 NPs, while the 11 nm sample transformed into hollow Co_3O_4 NPs. The 29 nm sample

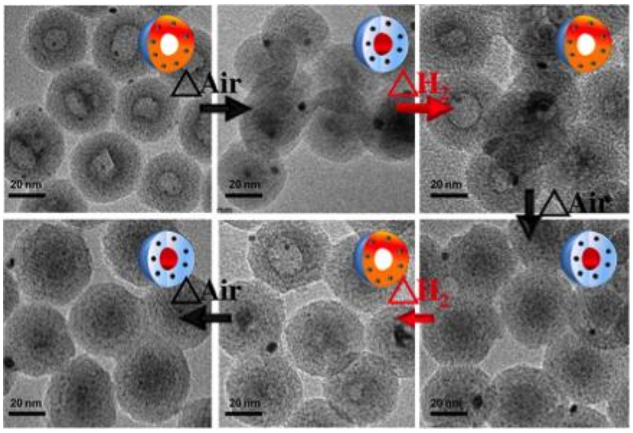

Fig. 3 Cyclic transformations of hollow $MnO-SiO_2$ NPs with small embedded Pt NPs into Mn_3O_4/SiO_2 core/shell NPs with small PtO NPs embedded in the shell by heating in air. Heating with H_2 drives the reverse reaction. Reprinted with permission from Reference 97. © 2013 American Chemical Society.

formed hcp-Co/Co_3O_4 core/shell NPs with a shell thickness of 3 nm. Higher temperatures were required to completely convert the 29 nm sample into hollow Co_3O_4 NPs. During the second reduction step, the 11 nm NPs were reduced to form Co/Co_3O_4 core/shell NPs, though the shell likely formed later, when the specimen was transferred into the TEM. The 29 nm hollow Co_3O_4 NPs fragmented into smaller NPs during the second reduction reaction.

Nakamura *et al*. investigated the reduction of hollow NiO and Cu_2O NPs by annealing under vacuum (5×10^{-5} Pa).[96] The voids collapsed as the reduced metal nucleated and grew. Hollow Cu_2O and NiO NPs underwent void collapse at 473 K and 623 K, respectively.

The studies discussed in this section thus far have used chemical reduction to drive morphological changes in NPs, including void collapse. Voids may also shrink in volume or collapse entirely in the absence of chemical reduction if hollow or porous nanostructures are heated to sufficiently high temperatures. Nakamura *et al*. also observed void shrinkage and collapse in hollow metal oxide NPs (for oxides of Fe, Ni, and Cu) while annealing in air, which would maintain an oxidizing atmosphere.[96,98] Void collapse is driven by vacancy diffusion to the nanostructure surface, which lowers the surface energy. The Gibbs-Thomson effect explains the mechanism of outward vacancy diffusion and void collapse in hollow NPs.[99–102]

In the same study discussed above, Nakamura *et al*. also observed shrinkage and void collapse of hollow CuO and NiO NPs when heating under air at higher temperatures of 673 K and 923 K, respectively.[96] Hollow CuO NPs were first obtained from oxidation of hollow Cu_2O NPs at 573 K, while maintaining their morphology. High-temperature annealing and collapse of Fe_3O_4, NiO, and CuO nanotubes under air was also reported.[98,103] The morphologies of hollow NPs and nanowires during void collapse resembled each other, but several significant details strongly depended on the composition. During the transformation of hollow Fe_3O_4 NPs or nanowires into γ-Fe_2O_3 through annealing, multiple small voids formed within the shell, which was attributed to outward diffusion of vacancies from the central void.[98]

3. Nanoparticle Phosphidation

Metal phosphide NPs can be obtained through reactions of metal NPs with reactive P-containing species. This section reviews recent advances in the synthesis of metal phosphide NPs.

A. Controlling Void Formation by Adjusting Reaction Conditions

While a common set of principles underpins the nanostructural transformations that accompany NP conversion chemistry, precise compositional and structural control remain challenging. Conversion chemical reactions have been controlled by varying the reactant concentrations, temperature and time, such that phase-pure products with controlled composition and morphology have been obtained for some systems. However, obtaining precise synthetic control remains challenging, and the reaction conditions need to be optimized for each system to account for different precursor chemistry, different nucleation and growth behaviour, and different products, especially where compounds of several compositions are available for some systems. Metal phosphide NPs have novel physical properties and have also served as a useful model system for understanding conversion chemistry.

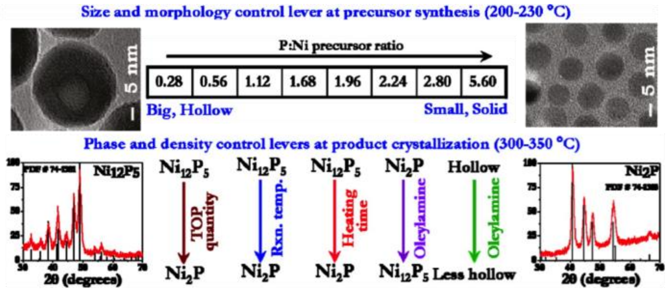

Fig. 4 Overview with inset TEM and XRD measurements of the chemical levers that control the composition, size, and morphology of Ni_xP_y NPs. Low P:Ni precursor ratios resulted in large, hollow NPs, while higher P:Ni precursor ratios gave small, solid NPs. Reprinted with permission from Reference 110. © 2011 American Chemical Society.

Muthuswamy *et al*. investigated the conversion of Fe NPs into phase-pure Fe_xP NPs.[104] Phase control was accomplished by conducting a series of reactions of Fe NPs with *n*-trioctylphosphine (TOP). TOP has been shown to serve as a P precursor for converting several kinds of metal NPs into metal phosphides.[105,106] The phase of the Fe_xP product was controlled by adjusting the reaction times, precursor concentrations, and sequence of addition: Phase-pure Fe_2P nanorods were favoured when the Fe NPs were reacted with TOP for short durations. As the reaction times were extended, the Fe_2P nanorods were incompletely converted into phases further enriched in P. Void formation through the Kirkendall effect was observed during partial conversion into FeP NPs. While phase-pure Fe_2P NPs were obtained at short reaction times, phase-pure FeP samples could not be obtained, even through prolonged heating. This inability to reach phase-pure FeP was attributed to formation of a FeP shell on the Fe_2P cores that inhibited further inward diffusion of P and outward diffusion of Fe. For synthesizing phase-pure FeP NPs, Fe NPs were combined with TOP that had been preheated to the phopshidation temperature of 350 °C. All of the FeP NPs produced in this manner had hollow cores, indicating formation via the Kirkendall effect.

Several studies have investigated control over the phase, size, and morphology of Ni_xP_y NPs. In the bulk, at least 8 phases of Ni_xP_y are known (Ni_3P, Ni_5P_2, $Ni_{12}P_5$, Ni_2P, Ni_5P_4, NiP, NiP_2, and NiP_3).[107] Chiang *et al*. and Henkes *et al*. independently showed that TOP serves as a P precursor during the formation of Ni_2P NPs.[108,109] While they observed void formation in some experiments and solid NPs in others, explicit detail of specific levers that controlled the morphology was not discussed. Wang *et al*. later demonstrated control over the formation or absence of voids by adjusting the P:Ni precursor molar ratio but obtained mixed $Ni_2P/Ni_{12}P_5$ (Ni_xP_y) compositions.[4] For P:Ni ≤ 3, Ni NPs were first obtained at 240 °C, which converted into hollow Ni_xP_y NPs at 300 °C via the Kirkendall effect. For P:Ni ≥ 9, amorphous Ni_xP_y NPs resulted at 240 °C, which converted into solid, crystalline Ni_xP_y NPs at 300 °C. Muthuswamy *et al.*[110] extended these ideas to obtain control over the NP composition. Phase-pure $Ni_{12}P_5$ and Ni_2P NPs were synthesized while adjusting parameters that determined the extent or absence of void formation. Ni_2P was favoured for higher temperatures (~300-350 °C), longer reaction times, and higher concentrations of TOP (Fig. 4).[110] The Kirkendall effect was also observed during formation of hollow Ni_2P NPs from large (~32 nm) Ni NPs. Smaller sizes

(~15 nm) did not undergo void formation during conversion into Ni_2P, which might arise from differences in the crystallinity of the different sizes. Compositional control was obtained by varying the amount of oleylamine. Large amounts yielded the more Ni-rich $Ni_{12}P_5$ phase, but also inhibited void formation, often resulting in solid $Ni_{12}P_5$ NPs. Muthuswamy *et al*. have also reported that Ni NPs can be converted into Ni_2P in a stepwise fashion, with $Ni_{12}P_5$ NPs as the intermediate.[111]

B. Effects of Precursor Reactivity

Precursors with different reactivity can also be used to control the morphology of the product NPs. Carenco *et al*. investigated the reaction of Ni, Cu, Fe, and Pd NPs with white phosphorous (P_4) to form metal phosphide NPs.[112] The higher reactivity of P_4 allowed for lower reaction temperatures, which is beneficial for large-scale production of NPs. Adjusting the reaction conditions including the metal:P ratio, temperature, and reaction duration resulted in different compositions, extents of crystallinity (amorphous vs. crystalline), and morphologies (*e.g.*, solid, hollow, core/shell, phase segregated). Ni and Fe NP templates yielded amorphous Ni_2P and FeP NPs at the lowest reaction temperatures. At higher reaction temperatures, the NPs became crystalline and had hollow cores as a result of the Kirkendall effect. Use of P_4 to obtain Fe-rich phases of Fe_xP_y was also investigated by increasing the precursor Fe:P_4 molar ratio. Double-shelled Fe_2P(interior)/Fe_xO_y(exterior) NPs with a central void were obtained when the ratio was increased to 16 Fe:P_4.

C. Observation of Intermediates

For some systems, a better understanding of the void formation process remains elusive, in part due to limited ability to observe intermediate stages before completion of the conversion reaction. While core/void/shell intermediates have been frequently observed for oxidation, many fewer intermediates are known during phosphidation. Ha *et al*. investigated the stepwise conversion of ε-Co (a metastable cubic structure commonly observed in Co NPs[113,114]) NPs into Co_2P and then into CoP NPs by reacting ε-Co NPs with TOP (Fig. 5).[115] During the conversion of ε-Co into Co_2P, inward diffusion of P atoms is initially faster than outward diffusion of Co. When a Co_2P shells crystallizes, however, outward diffusion of Co becomes more favourable, driving void formation. No additional voids were observed during conversion of Co_2P into CoP NPs, but the average size increased, which is suggestive of ripening. In a related study, Ha *et al*. investigated the oxidation of ε-Co NPs into CoO, followed by subsequent oxidation into Co_3O_4 NPs with air at 200 °C.[33] Conversion into hollow CoO NPs was complete after 30 minutes. After another 1.5 hours, CoO NPs were completely converted into Co_3O_4 NPs through outward diffusion of Co(II), resulting in enrichment in O. Both studies were accompanied by theory to better understand conversion mechanisms at the atomic scale.

4. Conversion into Metal Chalcogenides Using Cd Template Nanoparticles

Hollow metal chalcogenide NPs are of interest for their optical, magnetic, and electrochemical properties.[116–118] Precise morphological control of metal chalcogenide NPs obtained through conversion chemical reactions of metal NPs is highly desirable. Ibáñez *et al*.[119] investigated the morphological changes that occur when large (~300 nm diameter) spherical Cd NP templates react with O_2, elemental sulphur dissolved in *o*-dicholorobenzene (DCB:S), or with complexes of TOP and elemental sulphur, selenium, or tellurium (TOP:S, TOP:Se, and TOP:Te, respectively). The Cd template NPs were completely converted into CdO during the reaction with O_2, but no voids formed, suggesting that oxide anions diffused more quickly than Cd(II) (Fig. 6a). In the reaction with TOP:Se (TOP:Te), CdSe(Te) formed at both the shell/solution and Cd/CdSe(Te) core/shell interfaces (Fig. 6d,e). The shell thickness and crystallinity of the products were found to depend upon the relative chalcogenide and Cd NP concentrations.

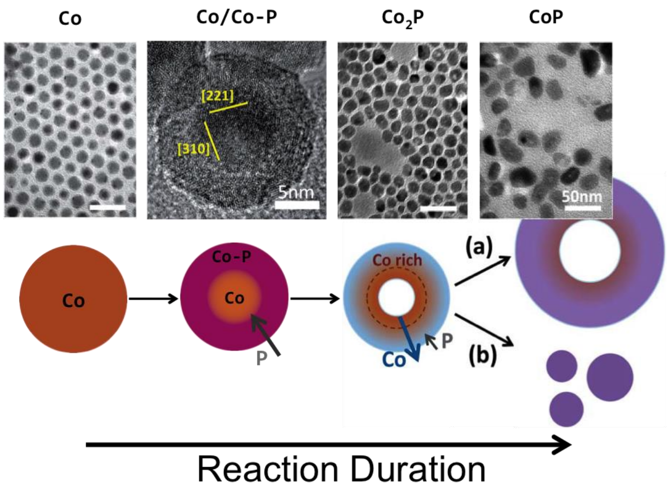

Fig. 5 Successive phosphidation reactions of Co NPs with TOP at elevated temperature. After formation of an amorphous Co-P shell, outward diffusion of Co results in hollow, crystalline Co_2P NPs. Further phosphidation into CoP can occur through two mechanisms: (a) The void size and outer diameter increase as a result of further outward diffusion of Co through the Kirkendall effect. (b) CoP NPs can fragment into smaller solid NPs, which may then grow into larger sizes through Ostwald ripening. Reprinted with permission from Reference 115. © 2011 Royal Society of Chemistry.

The amount of DCB:S allowed to react with Cd NPs was also varied. Large amounts of DCB:S (excess S) gave small crystal grain sizes and a large inner-to-outer radius ratio, which is close to the theoretical limit of nearly complete CdS shell growth at the shell/solution interface (Fig. 6b). Under these reaction conditions, outward Cd diffusion is much faster than inward S diffusion. The small grain size results from the fast nucleation of CdS grains at the CdS shell/solution interface. Smaller amounts of DCB:S gave reduced CdS nucleation rates, yielding larger crystal grain sizes and a small inner-to-outer radius ratio (Fig. 6c). The final structure is determined by the competition of conversion at the inner Cd/CdS core/shell interface and the outer CdS shell/solution interface. At high DCB:S concentrations, conversion occurs preferentially at the CdS shell/solution interface and is diffusion limited. At lower DCB:S concentrations, diffusion to the inner Cd/CdS core/shell interface becomes significant, and conversion is reaction limited. Hence, lower DCB:S concentrations promoted CdS growth at both the solution/CdS and Cd/CdS interfaces. The extent of void formation can also be controlled by adjusting the precursor reactivity. Hollow CdS NPs with a smaller inner diameter were also obtained when using TOP:S (Fig. 6c) in place of a small amount of DCB:S, because TOP:S is less reactive than DCB:S.

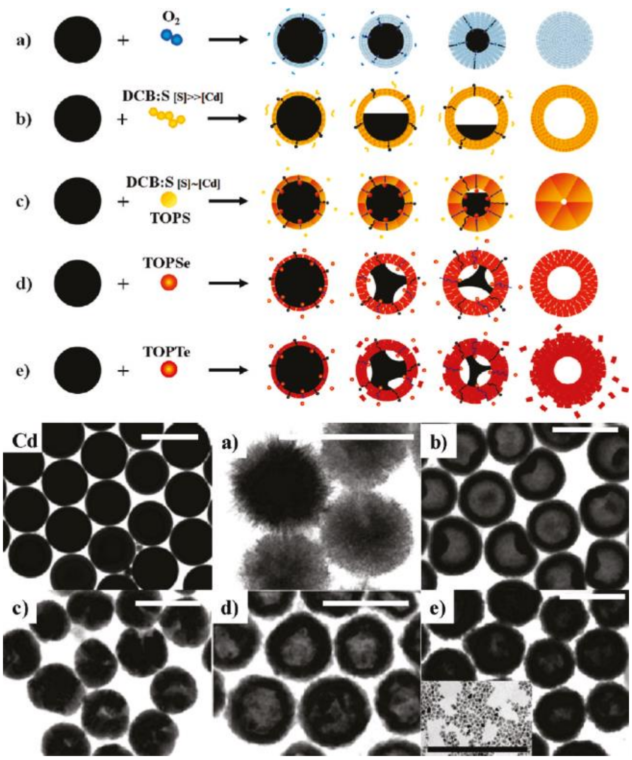

Fig. 6 Graphical representations and corresponding TEM images of the products for several conversion chemical reactions of large Cd NPs: (a) oxidation gives urchin-shaped CdO NPs, (b) a large excess of S in dichlorobenzene (DCB:S) produces hollow CdS NPs with a high inner:outer radius ratios, (c) smaller amounts of DCB:S or use of TOP:S drive formation of hollow CdS NPs with low inner:outer radius ratios, (d) TOP:Se produces hollow CdSe NPs, and (e) TOP:Te produces hollow CdTe NPs, as well as (e, inset) smaller solid CdTe NPs. All scale bars are 500 nm except for (e, inset), which is 100 nm. Reprinted with permission from Reference 119. © 2011 American Chemical Society.

5. Morphological Considerations During the Kirkendall Effect

A. Core and Void Geometry

Formation of voids together with remaining unreacted metal cores is well known as an intermediate for conversion chemical reactions of metal NPs that proceed through the Kirkendall effect. Analysis of the intermediate core/shell NPs gives greater insight into the Kirkendall effect. The metal core is usually attached to the shell in a symmetrical manner, such as being suspended by filaments, or in an asymmetrical manner, where the metal shares a common interface with the shell. In some instances, however, solid NP cores can be detached from the shell and completely surrounded by void space, giving the appearance of a “yolk/shell” NP with a floating yolk or a “nanorattle.” These possibile morphologies are depicted in Fig. 7. There is often insufficient information to unambiguously assign the morphology from TEM images because of resolution and contrast limits and the two-dimensional section provided by conventional TEM (unless tomography is performed). In many instances, the morphology can nevertheless be assigned with reasonable confidence.

The earliest examples of the Kirkendall effect in NPs showed several filaments connecting unreacted Co cores to the shells of CoSe or Co_9S_8 products.[13,51] Metal atoms diffuse along these filaments toward the shell by surface diffusion.[120] In this conversion mechanism, a string of voids appears at the core/shell interface. The voids may become connected in three dimensions as they grow. As the reaction proceeds, the void space increases, and the filaments grow longer and thinner. In two-dimensional images, the filaments appear to divide the void space into multiple voids, but if they are thin filaments, they simply penetrate through a single void space, in which the core is suspended (Fig. 7c). When the reaction is complete, the core and filaments have vanished because they have been incorporated into the shell.[121] This symmetrical conversion mechanism usually gives a symmetrical NP with uniform shell thickness because the core has diffused into all parts of the shell at the same rate.

In other systems, the core may be anchored to the inside of the shell in an asymmetrical manner, where there is a single void, and the core maintains a continuous interface adjacent to one part of the inside of the shell (Fig. 7a,b). In some systems, such asymmetric placement of the core results in non-uniform shell thickness,[43] but in other instances, the shell thickness can remain uniform.[119,122] This asymmetrical conversion mechanism may be attributed to the reduction in the surface energy when a single void forms, as compared with multiple voids and filaments for the symmetrical mechanism. Therefore, systems where filaments would exhibit particularly high surface energy might instead form an asymmetrical core and void, but kinetics are also critically important; diffusion must be fast enough on the time scale of the reaction to allow for reduction of the surface energy by effectively collapsing multiple smaller voids into a larger single void. Nakamura *et al*. discussed the differences in the symmetrical oxidation of Cu NPs and the asymmetrical oxidation of Ni NPs.[96] Railsback *et al*. investigated the size-dependent oxidation of Ni NPs and showed that small sizes (9 nm) form approximately symmetrical shells, yet partially oxidized intermediates show off-centre voids.[43] For these small sizes, most of the reaction occurs symmetrically through inward diffusion of oxygen before the Kirkendall effect drives asymmetrical void formation. For larger (26 nm) Ni NPs, asymmetry in the product is more prominent due to greater nonuniformity in shell thickness and because the larger size causes a high proportion of the overall oxidation reaction to occur asymmetrically through the Kirkendall effect. The morphology becomes asymmetrical once a void forms at the core/shell interface. Multiple voids form at the core/shell interface in larger (96 nm) Ni NPs because one void is no longer sufficient to serve as the source for vacancy diffusion throughout the NP. It should be noted that for fcc Co and Ni NPs of similar sizes (~10 nm), Co forms symmetrical shells and Ni forms asymmetrical shells, which highlights that composition and size both determine the morphology of intermediates and the final product.[13,43,50] The differences in diffusion behaviour might be attributed to faster diffusion at higher temperatures; Ni NPs were oxidized at higher temperatures (~300 °C) than Co (~150-200 °C).

Asymmetrical void formation also accompanies sulfidation of Cd NPs and oxidation of Bi NPs. During partial sulfidation of Cd NPs, asymmetric Cd/CdS core/shell intermediates with homogeneous shell thicknesses formed.[122] A recent study investigated oxidation of Bi NPs into Bi_2O_3, where Bi/Bi_2O_3 core/shell NP intermediates were observed using a liquid cell sample holder for TEM.[67] Two distinct behaviours were observed for individual Bi NPs: (1) After the initial stage of oxidation, a single Bi core was asymmetrically positioned on the inside of the Bi_2O_3 shell. Upon complete oxidation, the Bi_2O_3 shell that had been nearest to the Bi core was thicker than the section furthest from the core. (2) During oxidation, Bi exhibited liquid-like behaviour inside the void. In some NPs, the Bi core split into multiple Bi clusters. Upon complete oxidation, the Bi_2O_3 shell was locally thicker, where these Bi clusters had been deposited on the inside.

Yolk/shell structures with floating cores are the least well understood morphology obtained through the Kirkendall effect (Fig. 7d). We recently proposed that a yolk/shell structure may form from a core initially symmetrically connected to the shell through multiple filaments (Fig. 7c), if the filaments break before the core is completely consumed, causing the core to be left free-floating within the NP.[123] The yolk will still convert into the product, but without a clear outward diffusion path for metal atoms, inward diffusion may be favoured.[120] Henkes *et al*. reported yolk/shell structures for conversion of large Ni NPs into Ni_2P.[105] Sarac *et al*. have observed similar results for the conversion of Ni_3C_{1-x} NPs into $Ni_{12}P_5$.[123] In both studies, XRD measurements showed single-phase products, indicating the absence of Ni; therefore the floating core has been converted into the same material as the shell. Henkes *et al*. observed yolk/shell Ni_2P NPs, where some of the yolks were solid and others were hollow,[105] which is suggestive that the Kirkendall effect occurred again during the reaction of the yolk inside the outer shell.

B. Anisotroptically Shaped Nanoparticles and Assemblies

NP shape is another important lever for controlling diffusion and the Kirkendall effect. There is significant interest in anisotropically-shaped, hollow NPs. Before considering anisotropic shapes, we discuss the use of self-assembly to form chains of multifunctional magnetic metal NPs, which can be converted into nanowires. Such chaining is an example of “colloidal polymerization” of NPs, where each NP is analogous to a monomer that undergoes polymerization.[124,125] Combining conversion chemistry with NP self-assembly will also extend the capabilities of conversion chemistry to fabricate complex structures from NP assemblies.[126] Kim *et al*. prepared Co_3O_4 nanowires with Au inclusions by combining the Kirkendall effect with the attractive magnetic interactions of Co-based NPs.[127] Au/Co core/shell NPs, ~22 nm in diameter and capped with polystyrene (PS), were first synthesized. The size and Co content of these NPs cause them to spontaneously assemble into chains (even in the absence of an applied magnetic field), which were then oxidized and calcined into Au/Co_3O_4 nanowires. After annealing in air at 400 °C, the chains consisted of hollow Co_3O_4 NPs containing Au within the void spaces (Fig. 8). Different morphologies were obtained from annealing in air at higher temperatures (500-700 °C), where voids collapsed or were reduced in volume, and Au NPs were deposited on the outside of Co_3O_4.[128] As discussed in Section 2E, Nakamura *et al*. also observed collapse of hollow metal oxide nanostructures at high temperatures.[96,98,103] Keng *et al*. also obtained Co_3O_4 nanowires decorated with Pt, PtO, or PtO_2 by decorating chains of Co NPs with smaller Pt NPs.[129]

De Trizio *et al*. reported two methods for synthesizing Cu_3P hexagonal nanoplatelets.[130] In one method, spherical Cu NP templates were converted into Cu_3P hexagonal nanoplatelets by adding TOP. Intermediate Cu-Cu_3P NPs were obtained, which had a Janus morphology. In the second method, Cu_3P hexagonal nanoplatelets were synthesized directly from molecular precursors, suggesting a strong energetic preference for this structure.

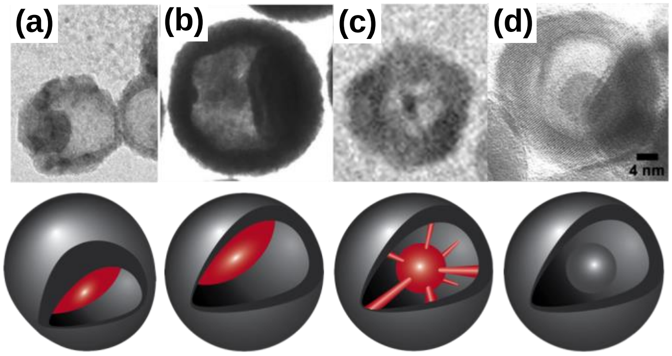

Fig. 7 (a-d) TEM images and graphical schematics below for different morphologies of NPs during or after conversion chemical reactions, where void formation occurs through the Kirkendall effect. (a) Ni/NiO core/shell NP, where the core is asymmetrically positioned on the inside of the shell, resulting in non-uniform shell thickness, (b) Cd/CdS core/shell NP, where the core is asymmetrically positioned on the inside of the uniformly thick shell, (c) Co/CoSe core/shell NP, where the core is suspended symmetrically within the void space by filaments extending from the core to the shell, and (d) Ni_2P yolk/shell NP displaying a core completely separated from the shell that floats freely within the void space. (a,b,d) reprinted with permission from References 43, 122, 105. © 2010, 2008, 2007 American Chemical Society. (c) Reprinted with permission from Reference 13. © 2004 American Association for the Advancement of Science.

Ren *et al*. investigated the oxidation of Ni nanowires of diameter 80 nm.[131] Below 550 °C (low-temperature regime), oxidation was driven primarily by the electric field gradient from adsorption of oxygen on the nanowire surface, characteristic of CM theory. At temperatures between 400-500 °C, NiO nanotubes formed through the Kirkendall effect, which were filled with alternating regions of solid Ni and void space. The quasi-periodic void arrangement likely served to reduce the surface energy in comparison with the possibility of many smaller voids. This result is consistent with the oxidation of spherical Ni NPs, where single voids are commonly observed at intermediate stages of oxidation rather than multiple voids.[43,66,96] In this low-temperature regime, oxidation became self-limiting when the tubular NiO shell reached a thickness of ~10-12 nm because the weaker electric field at greater thicknesses was insufficient to drive further oxidation. A related study on the oxidation of Cu nanowires reported a similar morphology during partial conversion into CuO nanotubes.[132]

Subsequent heating of Ni nanowires at temperatures above 550 °C (high-temperature regime) gave complete oxidation of the Ni nanowire templates, where the Ni segments within the NiO nanotubes diffused out through the sidewalls and were deposited as NiO on the outer surface.[131] The sidewalls of the completely oxidized product had quasi-periodic variations in thickness and outer diameter because they were thicker in the regions that had been adjacent to the Ni segments at lower temperatures.

Conical NPs are also of interest for their distinct, asymmetry. Jeong *et al*. fabricated SnO_x nanocone arrays supported on glass or Si by oxidizing Sn islands that had been deposited by electron beam evaporation.[133] Oxidation was conducted at elevated temperatures (~220-450 °C) under different O_2 partial pressures (P_{O2}). For $P_{O2} \leq 100$ ppm, solid SnO_x nanocones formed. In this regime, the Sn islands melted, and oxidation occurred first at the base and then through the volume of each island, giving solid nanocone products. At P_{O2} > 100 ppm, SnO_x hollow nanoislands formed. A SnO_x layer

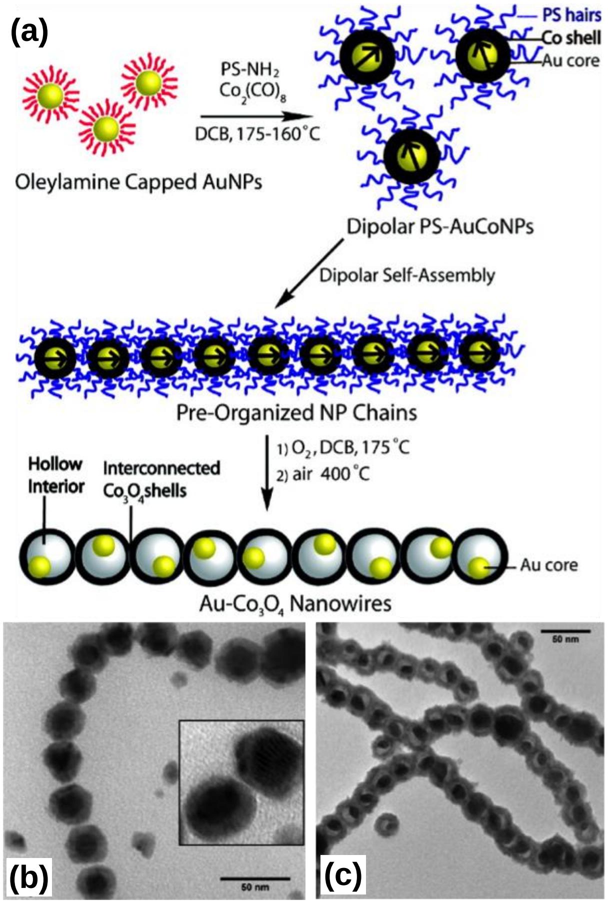

Fig. 8 (a) Graphical schematic showing the process for synthesizing Au/Co core/shell NPs, assembling them into chains, and converting them into Au/Co_3O_4 nanowires. TEM images of chained (b) Au/Co core/shell NPs and (c) Au/Co_3O_4 core/shell NPs, where Au is located asymmetrically within the voids formed during oxidation of Co into Co_3O_4. Reprinted with permission from Reference 127. © 2010 American Chemical Society.

quickly formed, and oxidation was accompanied by the Kirkendall effect, resulting in hollow SnO_x nanoislands. Varying the reaction conditions can profoundly affect the structure of the reaction products.

Sun *et al*. fabricated hollow ZnS nanoneedles via the Kirkendall effect driven by anion exchange (Section 8), but this study is discussed here because of the anisotropic shape of the NPs.[134] Solid ZnO nanocones were converted into hollow ZnS nanoneedles through a reaction with thioacetamide. The conical shape of the ZnO template NP imparted control over the location and shape of the void. At low reaction temperatures, multiple voids formed at the core/shell interface, leaving several bridges of material located between the ZnO core and the ZnS shell. At higher reaction temperatures, faster diffusion allowed coalescence of the smaller voids into a larger void at the apex of the nanocones. As sulfidation proceeded, the void grew away from the apex and toward the base of the nanocone, until the final ZnS product had an open-ended base with access to the interior, thus completing conversion into a nanoneedle.

C. Void Formation through Selective Etching of Multimetal Nanoparticles

There have been several reports of void formation in multimetallic NPs containing Pt mixed with transition metals,[135] where the transition metal is removed through selective etching. These NPs can be used as catalysts for the oxygen reduction reaction (ORR) in proton exchange membrane fuel cells (PEMFCs). PEMFCs operate at low temperature (~70 °C) and near ambient pressure. The chemical, structural, and catalytic properties of Pt_3Co NPs incorporated into PEMFCs were recently investigated.[136,137] In a typical setup, carbon-supported Pt and Pt_3Co NPs are loaded onto anodic and cathodic membranes, respectively. Humidified air is fed into the cathode, and dry H_2 is fed into the anode. After running a stack of PEMFCs at constant current density (typically for times longer than one month), a NP sample can be collected from the cathode for analysis. The Co or Ni portion of the NP can be leached away, leaving a Pt-enriched nanostructure behind, which may be facilitated if the Kirkendall drives outward diffusion of Co or Ni toward the NP surface. For example, monocrystalline Pt_3Co NPs were converted into four different NP morphologies, hollow Pt, solid Pt, hollow Pt-Co, and Pt/Co core/shell NPs.[138] Pt_3Ni polyhedra have also been converted into Pt_3Ni nanoframes with Pt-enriched surfaces.[139]

The mechanism for dissolving Co or Ni has yet to be fully clarified. If Co or Ni diffuses to the NP surface prior to removal though oxidative etching, the remaining nanostructure can be significantly enriched in Pt. In this case, void formation would be driven by the Kirkendall effect. Alternatively, formation of pinholes could allow for more direct dissolution, which was recently modelled for core/shell NPs containing transition metal cores.[140] In this model, fluctuations of the NP shape can cause frequent opening and closing of pinholes in the Pt-rich shell, which allows for reactive species to penetrate into and to etch the NP core from within. Additional studies are needed to further discern the mechanism of Co or Ni removal. For example, more detailed observations of intermediate stages of void formation and compositional changes in the Pt-rich shell may help to determine the mechanism.[141]

6. Void Formation through Solid-State Diffusion Couples

While the Kirkendall effect has commonly been observed for reactions of metal NPs with non-metals, reactive metals can also react with metal NPs. Jana *et al*. reported formation of hollow intermetallic $NiZn_x$ NPs through the reaction of Ni NPs with diethylzinc at 250 °C.[142] Deposition of Zn drove outward diffusion of Ni, forming $NiZn_x$. Galvanic exchange (Section 7) was ruled out as a possible conversion mechanism.

Anumol *et al*. conducted *in situ* TEM studies of the formation of hollow intermetallic PtBi NPs.[143] A solution containing H_2PtCl_6 and Bi(acetate)$_3$ was microwave heated at 100 °C. Initially, small Pt NPs grew and formed larger aggregates (Fig. 9b). Bi_2O_3 sheets formed and encapsulated the aggregates of Pt NPs (Fig. 9c). Small Bi NPs formed within the Bi_2O_3 sheets (Fig. 9d). Pt then diffused outward, resulting in hollow or porous PtBi NPs (Fig. 9e). These results were attributed to outward diffusion of Pt driven by the high surface energy of the small Pt NPs within the aggregates. The Kirkendall effect was not suspected because Pt has slower self-diffusion than Bi, though the diffusion rates of Pt and Bi in PtBi were not discussed.

7. Recent Advances in Galvanic Exchange Reactions

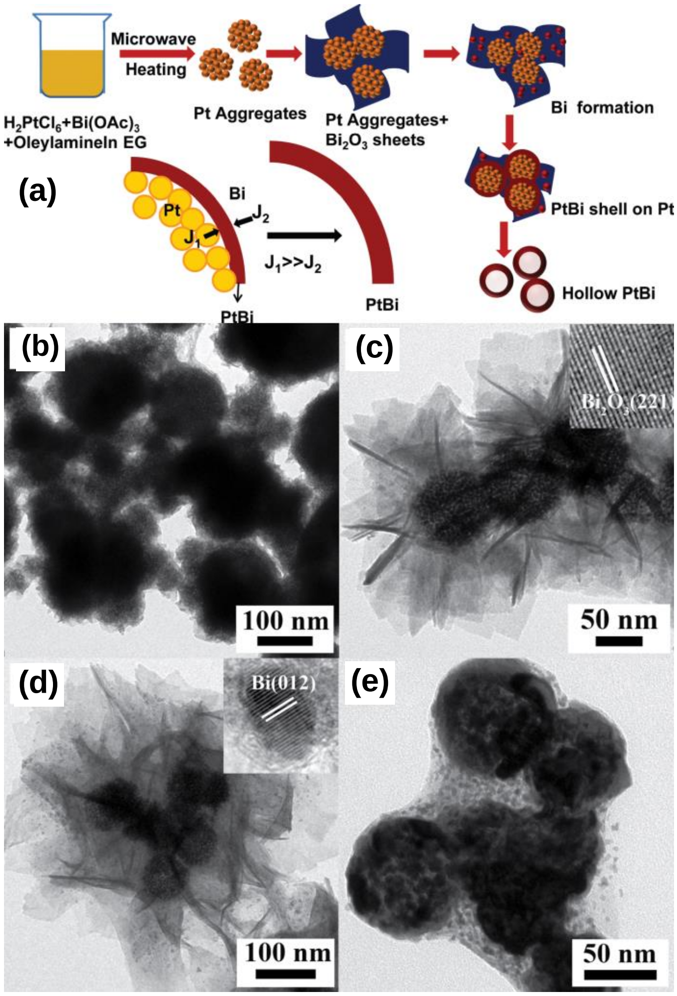

Fig. 9 (a) Graphical schematic depicting the stepwise formation of hollow PtBi NPs and TEM images showing (b) aggregates of Pt NPs, (c) Bi_2O_3 sheets surrounding the Pt NP aggregates, (d) Bi NPs formed within the Bi_2O_3 sheets, and (e) hollow or porous PtBi NPs. Reprinted with permission from Reference 143. © 2013 WILEY-VCH Verlag GmbH & Co. KGaA, Weinheim.

Galvanic exchange reactions are commonly employed for obtaining NPs with complex morphologies, particularly for hollow nanostructures of controlled compositions and porosity. This section is focused on the most recent developments and understanding in controlling galvanic exchange reactions. We also direct the reader to a recent review on galvanic exchange.[144]

Galvanic exchange reactions rely on the different reduction potentials of two elemental metals, which combine to give a favourable redox reaction. Atoms of a more easily oxidized metal (having a lower reduction potential) in the template NP oxidize and dissolve into solution, thus sacrificing the template NP (Scheme 1b). Ions of a more noble metal (having a higher reduction potential) are simultaneously reduced onto the template NP. Galvanic exchange reactions begin with deposition of the more noble metal and an alloying process, where it is alloyed into the template NPs. As deposition and alloying of the more noble metal proceeds, dissolution of the less noble metal drives pinhole formation. Pinholes serve as sites, where template metal atoms oxidize and dissolve into solution. Electron tunnelling allows pinholes to form in the locations where they are most stable; the pinholes do not have to form adjacent to where the more noble metal is reduced and deposited onto the NP. The resulting cavity expands toward the centre of the NP, causing dissolution from the inside out. Dealloying becomes the predominant process as the reaction continues, which is exemplified by selective oxidation and dissolution of the template metal. Dealloying can result in fragmentation, collapse, or breakup of the converted NP shell or frame.[145,146] In order to avoid the destructive effects of dealloying, galvanic exchange reactions often are not run to completion. Enrichment of the more noble metal through galvanic exchange drives both alloying and dealloying; the distinction is that alloying describes initial formation of pinholes and larger voids, while dealloying is a more local effect, where the remaining less noble metal atoms are removed.

Since noble metals have high reduction potentials, galvanic exchange reactions are often conducted using noble metal salts, where common products are Au, Pd, and Pt. Ag nanostructures have often been used as sacrificial templates for galvanic exchange reactions, and Cu, Al, Ni, and Co, have also been demonstrated as template materials.[147–151] Structures commonly obtained through galvanic exchange include NPs, nanocages, nanorods, nanotubes, nanorattles, nanoframes, and nanobowls.[14,19,152–159]

A. Controlling the Final Morphology of Galvanic Exchange Products

The morphology of galvanic exchange products depends on the size and shape of the template NPs and can also be controlled by adjusting the reaction conditions. Galvanic exchange reactions are often conducted in aqueous solutions because Ag template NPs with well-controlled shapes are usually synthesized in aqueous solutions. Zhang *et al.* conducted a series of galvanic exchange reactions on Ag nanocubes to form PtAg bimetallic NPs of various morphologies through reactions with K_2PtCl_4 (Fig. 10).[160] Pt was deposited onto the surfaces of Ag nanocubes while Ag^+ ions formed $AgCl_{(s)}$. HCl and polyvinylpyrrolidone (PVP) were also added to impart morphological control over the PtAg products. HCl regulated the reaction kinetics by facilitating precipitation of $AgCl_{(s)}$ onto the NP surface, which served as a nucleation site for deposition of Pt. At low HCl concentrations, $AgCl_{(s)}$ was limited to one nucleation site (typically one of the corners or sides of the Ag nanocubes). At higher HCl concentrations, $AgCl_{(s)}$ formed more quickly and at multiple sites. In recent work by González *et al.*, addition of ascorbic acid was shown to prevent AgCl deposition and gave access to another reaction regime, where sequential galvanic exchange and the Kirkendall effect yielded hollow AgAu NPs with double-walled and other complex morphologies.[161] This combination of galvanic exchange and the Kirkendall effect was used to synthesize cubic, spherical, and cylindrical NPs.

AgAu is a common system for galvanic exchange, where solid Ag NPs are converted into hollow or cage-like AgAu alloy NPs, whose morphology is dictated by the shape of the Ag template NPs. Chien *et al.*[162] have performed a subsequent ripening step on hollow AgAu alloy NPs to fill the void spaces while preserving the overall shape, thus allowing conversion of Ag NPs of various shapes (*e.g.*, nanoplates, nanodecahedrons, nanorods, nanoprisms, nanospheres, and thin films of thickness < 10 nm – 5 μm) into solid Au NPs of the same shape as the Ag template NP. Use of ascorbic acid (AA) and cetyltrimethylammonium bromide (CTAB) in conjunction with $HAuCl_4$ is necessary to preserve the morphology of the initial

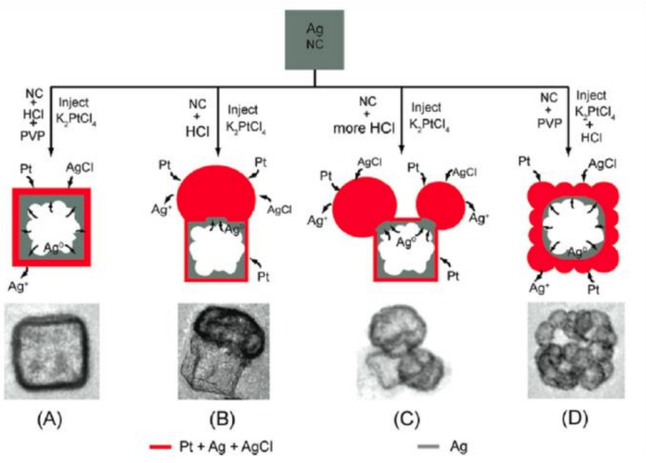

Fig. 10 Graphical schematic and TEM images acquired for galvanic exchange reactions of Ag NPs with K_2PtCl_4 in the presence of HCl under different reaction conditions, resulting in (a) nanoboxes, (b) heterodimers, (c) multimers, and (d) popcorn-shaped NPs. Reprinted with permission from Reference 160. © 2012 American Chemical Society.

Ag template NP. Complexation of CTAB with Au(III) is thought to mediate the reduction rate, imparting kinetic control over Au deposition into the hollowed AgAu NPs. AA controls deposition of Au; as a mild reducing reagent, it may provide an alternative route for reduction than galvanic exchange.[163]

Pradhan *et al*. synthesized highly branched Au nanoflowers resembling carnations, which have sharp tips created through galvanic exchange.[164] Galvanic exchange was performed on Cu NPs embedded in negatively-charged polystyrene beads, where formation of sharp Au tips rather than flat layers was attributed to a polarization effect between Cu(0) and $AuCl_4^-$ that directed deposition into tips. Such sharp Au tips are of special interest for surface enhanced Raman scattering (SERS).[165]

B. Galvanic Exchange Reactions in Organic Solvents

Karvianto *et al*. investigated the size dependence of galvanic exchange of Ag NPs in solutions of octadecene, oleylamine, and toluene through addition of $HAuCl_4$.[166] Larger (~43 nm) Ag NPs converted into hollow AuAg alloy NPs, and smaller (~20 nm) Ag NPs first formed hollow AuAg alloy NPs, followed by dealloying and void collapse. Octadecene and oleylamine were thought to sterically hinder diffusion of $HAuCl_4$ to the surface of the template NPs, resulting in formation of hollow AuAg alloy NPs, whose shell thickness was proportional to the concentration of $HAuCl_4$. After nearly complete oxidation of Ag with $HAuCl_4$, oleylamine likely reduces $HAuCl_4$, driving deposition of Au and alloying into the NPs as the $HAuCl_4$ concentration is increased. Therefore, to the extent that oleylamine drives reduction of $HAuCl_4$, dealloying of Ag^+ into solution would also be suppressed. Oleylamine may also dissolve $AgCl_{(s)}$, preventing its deposition onto the NP surface. The smaller Ag NPs shrank in size during galvanic exchange in oleylamine, but the larger NPs grew because oleylamine also drove reduction of Au^+ and its deposition onto the NPs. This example highlights the significance of size in galvanic exchange and reduction reactions.

More recently, Polavarapu and Liz-Marzán developed a method for synthesizing Ag nanocubes and converting them into AgAu nanocages in *o*-dichlorobenzene/toluene mixtures by adding $HAuCl_4$ and using oleylamine as a ligand and reducing agent.[167] Since oleylamine can serve as a reducing agent, Au can also be deposited onto Ag NPs[168] or Ag onto Au NPs[169] by reduction rather than galvanic exchange, giving AgAu alloy NPs after annealing.

The crystallinity and morphology of galvanic exchange products are often determined by the crystallinity of the template NPs.[20,170] Therefore, levers that control the crystallinity and morphology of the template NPs (such as solvents, ligands, reagent concentrations, and temperature) can be critically important for determining the outcome of galvanic exchange reactions.[171,172]

C. Templates of Different Compositions

Reactions of Ag template NPs with Au or Pt salts for galvanic exchange reactions have been popular due to the ability to readily obtain Ag NPs of different sizes and shapes. The nobility of Au and Pt also provides significant thermodynamic driving force for galvanic exchange reactions. This section discusses other kinds of template NPs and metal salts that have been employed in galvanic exchange reactions.

Niu *et al*. investigated galvanic replacement of highly reactive Mg and Zn template NPs with Ag^+, $AuCl_4^-$, Cu^{2+}, and Sn^{2+} oxidants to form porous Ag, Au, Cu, and Sn NPs.[173] Special measures are required to prevent or control oxidation of such reactive template NPs. Spherical Al NPs have been shown to serve as templates for galvanic exchange reactions forming Co, In, Fe, Au, Ag, Cu, Pt, Pd, and Pb porous nanostructures.[150,151] Cu NPs have also been used as template NPs in galvanic exchange reactions. Xie *et al*. investigated the galvanic conversion of Pd/Cu core/shell nanocubes into Pd/M_xCu_{1-x} (M = Au, Pd, and Pt) yolk/shell nanocages.[174,175] Cu nanocubes and nanowires have also been converted into hollow Au_xCu_{1-x} nanocubes and nanotubes with porous sidewalls, respectively.[176] Mohl *et al*. converted Cu nanowires into CuPd and CuPt bimetallic nanotubes through reactions with Pd and Pt salts.[157] Other template materials include Ni and Co NPs, which can be converted into hollow noble metal nanorods or NPs.[177–180]

Oh *et al*. recently reported galvanic exchange reactions on Mn_3O_4 nanocubes using $Fe(ClO_4)_2$.[181] Fe(II) was oxidized to Fe(III) and deposited onto the Mn_3O_4 nanocubes as γ-Fe_2O_3. Meanwhile, Mn(III) in Mn_3O_4 was simultaneously dissolved into solution as it was reduced to Mn^{2+}, which facilitated dissolution of Mn_3O_4, yielding γ-Fe_2O_3 nanocages (Fig. 11). The Kirkendall effect and cation exchange were ruled out as possible conversion mechanisms because the reaction was conducted at a relatively low temperature (90 °C), at which diffusion of Mn and Fe would be slow. At low $Fe(ClO_4)_2$ concentrations, the Mn_3O_4 core was partially dissolved, and a hole began to form in the centre of the solid Mn_3O_4 NP. At higher $Fe(ClO_4)_2$ concentrations, reductive dissolution of Mn_3O_4 was more prevalent as γ-Fe_2O_3 was deposited first onto the exterior and then inside of the template nanocubes, forming nanocages. This process allows for nearly complete conversion of solid Mn_3O_4 NPs into hollow γ-Fe_2O_3 NPs. In the same study, galvanic replacement reactions of Co_3O_4 and Mn_3O_4 nanocubes with $SnCl_2$ produced hollow or porous Co_3O_4/SnO_2 and Mn_3O_4/SnO_2 nanocages, respectively.

8. Anion Exchange

Anion exchange is a growing subfield of conversion chemistry, where anions within multicomponent NPs are exchanged (Scheme 1c). During anion exchange, NPs often undergo morphological changes through the Kirkendall effect.

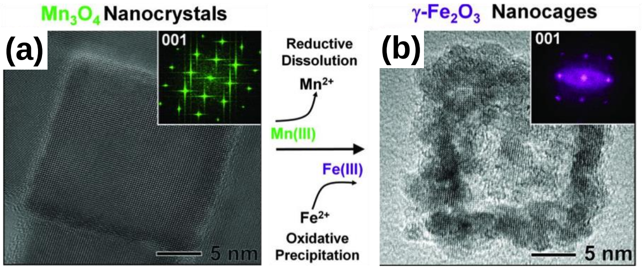

Fig. 11 TEM images showing galvanic exchange in oxide NPs: (a) starting Mn_3O_4 nanocubes and (b) the γ-Fe_2O_3 nanocage product. Reprinted with permission from Reference 181. © 2013 American Association for the Advancement of Science.

Anions generally diffuse more slowly than cations due to the larger size of anions. Slow anion diffusion often requires longer reaction times and higher temperatures than cation exchange. The slow reaction kinetics of anion exchange can be advantageous for obtaining control over intermediate products with partial anion exchange.[182] In cation exchange, the smaller cations can often diffuse readily through the template NP, which preserves the anion sublattice. Consequently, cation exchange is often templated by the anion sublattice, which leaves the NP morphology unchanged. During anion exchange, however, diffusion of cations is often promoted, thereby disrupting the cation sublattice and causing major morphological changes. Cation exchange has recently been comprehensively reviewed elsewhere.[26,183] Therefore, anion exchange is reviewed here.

In principle, a thermodynamic framework can be constructed for anion exchange that is similar to cation exchange, where the Gibbs free energy for cation exchange reactions is determined by the Gibbs free energies of formation for the compounds and the reduction potentials of the cations.[25] The reduction potentials of the molecular precursors for the incoming anions and the oxidation potentials of the outgoing anions would need to be considered to adapt this framework to anion exchange, which is challenging because the reduction potentials of the molecular precursors vary for each precursor, and the outgoing anions often undergo further reactions, such as O^{2-} into OH^-. Therefore, the source of incoming anions and the successive reactions of outgoing ions are important for determining thermodynamic spontaneity. The law of mass action may also be used to drive reactions forward that would not be favourable in their standard states by increasing the concentration of some reagents, as is known for cation exchange.[184] For example, metal oxides generally have more negative Gibbs free energies of formation than the corresponding sulphides,[41] but reactions associated with the anions and the concentrations can tip the energy balance to make sulfidation of oxides favourable.[185–188] Indeed, metal oxides are an attractive precursor for anion exchange reactions due to their stability (as compared with reduced metals, which are susceptible to oxidation), provided that they are not too stable to undergo anion exchange. There are also examples, however, of metal oxides failing to undergo anion exchange.[109,187,189]

Park *et al*. reported anion exchange of solid, monocrystalline ZnO NPs into hollow, monocrystalline ZnS NPs.[6] In the case of partial anion exchange, hollow ZnO/ZnS core/shell NP were obtained, where ZnO bridges connected the ZnO core to the ZnS shell, while maintaining an epitaxial interface despite large lattice mismatch (Fig. 12). Huang *et al*.[190] also observed epitaxial growth of ZnS on monocrystalline ZnO nanorod arrays. TEM revealed homoepitaxial growth of ZnS through anion exchange, where voids formed as ZnO was consumed and ZnS was simultaneously produced. Furthermore, the hexagonal cross-section of the ZnO nanorods was preserved, with minor warping, to produce monocrystalline ZnS nanorods. In another study, addition of ammonium sulfide ($(NH_4)_2S$) to hollow CoO NPs at 70 °C drove formation of hollow, amorphous Co-S NPs. The high reactivity of $(NH_4)_2S$ allowed for low-temperature anion exchange. Subsequent annealing at 200 °C drove formation of hollow, polycrystalline Co_3S_4 NPs with larger void spaces, indicating further outward diffusion of Co.[191]

Anion exchange has also been demonstrated in Sn-based nanostructures. Cai *et al*. performed a stepwise reaction, successively transforming Zn_2SnO_4 nanooctahedra into SnO_2 and then into SnS_2 using ethylenediaminetetraacetic acid (H_4EDTA) to extract Zn^{2+} and thioacetamide as a sulphur precursor.[192] Sines *et al*. reported anion exchange reactions in the conversion of monocrystalline SnSe nanosheets into SnTe.[193] SnTe grew epitaxially on the SnSe nanosheets, accompanied by void formation. The porous product consisted of a pattern of SnTe nanocubes and nanobars with specific crystal orientations separated by void space. Anion exchange has also been demonstrated in the conversion of nanosheets of Co_3O_4 into CoS, NiO into NiS, and WO_3 into WS_2.[194,195]

The examples discussed thus far have involved anion exchange of inorganic template nanostructures into metal compounds of various compositions. There is also interest in using organic-inorganic hybrid nanomaterials as starting materials for anion exchange reactions. For example, Xiong *et al* conducted anion exchange on solid Cu_2O/PVP hybrid NPs (PVP NPs containing crystallites of Cu_2O) through a reaction

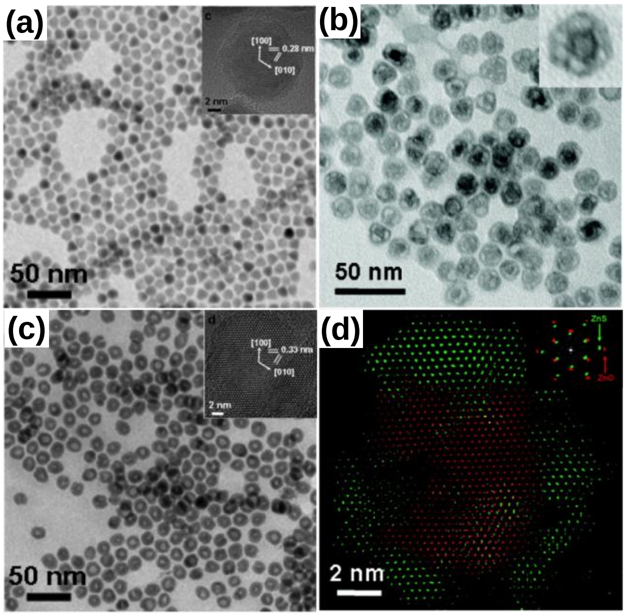

Fig. 12 TEM images acquired at different stages of anion exchange of ZnO NPs with hexamethyldisilathiane, resulting in ZnS NPs: (a) solid ZnO NPs with HRTEM inset, (b) partial anion exchange products, ZnO/ZnS core/shell NPs with prominent voids formed through the Kirkendall effect, and (c) hollow ZnS NPs obtained after complete anion exchange with HRTEM inset. (d) Reconstructed image from fast Fourier transform (FFT) spots showing heteroepitaxial growth of ZnS onto ZnO during partial anion exchange. Alignment of the spots in the inset FFT confirms epitaxy. Reprinted with permission from Reference 6. © 2009 American Chemical Society.

with thiourea, converting them into hollow, concentric multishelled Cu_2S NPs.[188] PVP slowed diffusion of thiourea to the Cu_2O NP surface and allowed for outward diffusion of Cu to drive formation of a Cu_2S shell surrounding the hybrid core. Formation of multiple Cu_2S shells was attributed to densification of Cu_2S during the anion exchange reaction (Fig. 13). Multishelled Cu_2S NPs were synthesized with control over the number and thickness of the Cu_2S shells by adjusting the reaction conditions, precursor concentrations, and capping agents.

Organic-inorganic templates containing organic rather than elemental metal cations may be particularly suitable for anion exchange because the larger size of organic cations may facilitate anion diffusion. Two studies reported anion exchange of $(Fe_{18}S_{25})(TETAH)_{14}$ (TETAH = protonated triethylenetetramine) layered nanoribbons, sheets of $Fe_{18}S_{25}$ separated by TETAH.[196,197] $(Fe_{18}S_{25})(TETAH)_{14}$ thermally decomposes into Fe_7S_8 nanowires under an argon atmosphere due to desulfurization and loss of TETAH.[196] Thermal decomposition in air resulted in porous α-Fe_2O_3 nanorods.[196] TOP has been demonstrated to extract Se and S from metal chalcogenide NPs by forming TOP:Se and TOP:S complexes.[198] TOP can also release P and drive phosphidation, as described in Section 3. The reaction of $(Fe_{18}S_{25})(TETAH)_{14}$ nanosheets with TOP yielded porous FeP nanosheets.[197] The porosity of the FeP nanosheets was attributed to lattice strain release from lattice mismatch and dissolution of TETAH rather than the Kirkendall effect. MoO_3-EDA (EDA = ethylenediamine) nanowires have been reported to undergo anion exchange with L-cysteine to form hierarchical nanosheet-based MoS_2 nanotubes, where the nanotube walls were composed of MoS_2 nanosheets.[199] Elevated reaction temperatures drove dissolution of EDA and decomposition of L-cysteine, which simultaneously donated S^{2-} and consumed O^{2-}.

Anion exchange accompanied by the Kirkendall effect has been observed in several rare-earth-based NPs, where the large cation size may help facilitate anion exchange. Rare-earth-based NPs exhibit unique optical and magnetic properties, which are appealing to combine with hollow morphologies.[200–208] Zhang *et al.* reported the Kirkendall effect during anion exchange reactions of solid Y_2O_3 NPs with NaF and HF into hollow α-$NaYF_4$.[209] Hollow LaF_3, $LaCO_3F$, and GdF_3 NPs have also been obtained through anion exchange.[210,211] Hollow $GdPO_4$ NPs were synthesized through anion exchange of solid $Gd(OH)CO_3$ NPs with $NH_4H_2PO_4$, which served as the PO_4 precursor.[212,213] Reactions of $Y(OH)CO_3$ and $Gd(OH)CO_3$ NPs with NH_4VO_3 gave hollow YVO_4 and $GdVO_4$ NPs.[203,214] Hollow $Yb(OH)CO_3/YbPO_4$ core/shell NPs were also synthesized from solid $Yb(OH)CO_3$ template NPs and $NH_4H_2PO_4$.[200] Some general trends should be noted about anion exchange reactions on rare-earth-based template NPs: The product NPs typically have an urchin-like morphology, where the NP surface is rough. Conversion intermediates usually have symmetric core/shell structures, where the core is suspended by filaments that serve as diffusion pathways to consume the core (Section 5).

While most studies of anion exchange have utilized metal oxide, organic-inorganic hybrid, or rare-earth-based template NPs, anion exchange of metal chalcogenide semiconductor NPs has also been reported. For example, partial anion exchange of spherical wurtzite (w)-CdS NPs has been demonstrated. Phase-segregated w-CdS/zb-CdTe heterodimers (zb = zinc blende) formed through a reaction with TOP:Te.[182] Epitaxial growth of zb-CdTe from w-CdS NPs coupled with type-II band alignment allows for oriented separation and transfer of charge carriers in the heterodimer during photoexciation.[215] Minimal anion exchange occurred, however, when TOP:Se was added to CdS NPs at elevated temperature, which was attributed to the stronger affinity of TOP for Se than Te.[182]

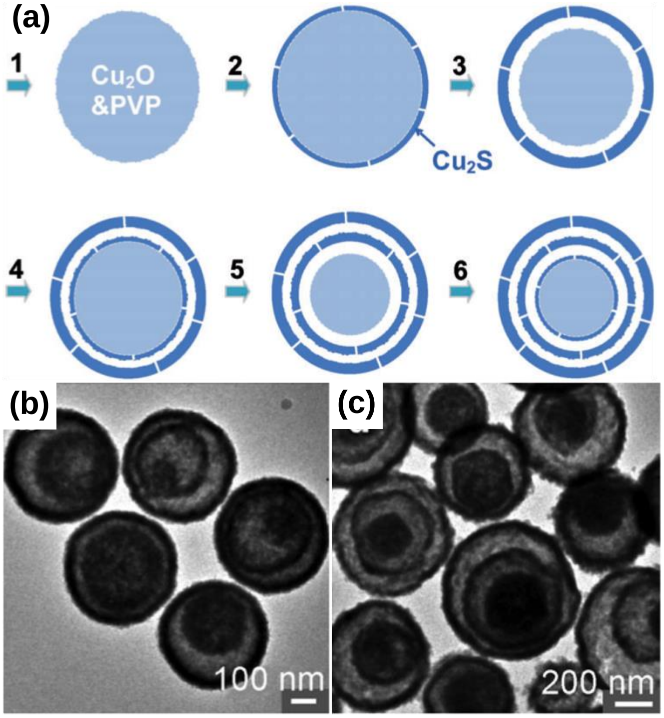

Fig. 13 (a) Graphical schematic depicting stepwise formation of multishelled Cu_2S hollow NPs through anion exchange at 220 °C. TEM images of (b) double-shelled particles and (c) a mixture of double- and triple-shelled NPs. Reprinted with permission from Reference 188. © 2012 WILEY-VCH Verlag GmbH & Co. KGaA, Weinheim.

9. Selective Conversion Chemical Reactions in Multicomponent Nanoparticles

NPs containing multiple chemically distinct domains can undergo selective conversion chemical reactions, where only one or some of the domains react with a particular reagent. Such selective conversion reactions can be used to tailor the composition and morphology of heterostructured NPs. For example, when noble metal/transition metal core/shell NPs undergo the Kirkendall effect, voids form at the noble metal/transition metal compound interface, but the pattern of the voids can vary. In the first report of the Kirkendall effect in NPs, Pt/Co core/shell NPs were oxidized into Pt/CoO core/shell NPs.[13] The Pt cores retained their catalytic activity for ethylene hydrogenation reactions, which indicated that the CoO shell was sufficiently porous to allow transport of the reactants and products. In another study, elemental Fe was deposited onto Au NPs, which were oxidized to form Au/iron oxide core/shell NPs.[216] FePt/Co core/shell NPs have also been converted into $FePt/CoS_2$ core/shell NPs by adding elemental sulphur.[217]

Assembling higher-order heterostructured colloidal NPs using a multistep processes is conceptually analogous to total synthesis of complex molecules from simple building blocks, where a vast toolbox of reactions can give complex structures.[218] Buck *et al*. have outlined a total synthesis approach for constructing heterostructured NPs.[219] For example, heterotrimers were formed by crosslinking individual NPs with a third bridging material, while heterotetramers were obtained from heterogeneous nucleation and growth of an additional compositionally distinct domain onto heterotrimers. They also reported sulphur-mediated formation of heterooligomers through selective coupling of Au domains between pairs of Au-Pt-Fe_3O_4 heterotrimers.

Hill *et al*. developed a multistep synthesis for depositing Co onto the tips of Pt-tipped CdSe/CdS core/shell quantum dot nanorods (QDNRs).[220] Co NP growth at the tips of QDNRs was assisted by Pt nuclei that had been deposited on the tips in a previous step. Bubbling O_2 through the solution at elevated temperature selectively oxidized Co, resulting in hollow CoO NPs through the Kirkendall effect, while leaving the Pt, CdSe, and CdS domains of the heterostructured NP unaffected.

Bradley *et al*.[221] investigated conversion chemical reactions of Pt-Fe_3O_4 heterodimer NPs with $Pb(acac)_2$ (acac = acetylacetonate) and $Sn(acac)_2$. Both metal salts selectively converted the Pt domain into intermetallic PtPb or a Pt_3Sn alloy, yielding PtPb-Fe_3O_4 or Pt_3Sn-Fe_3O_4 heterodimer NPs with sharp compositional interfaces. Furthermore, PtPb-Fe_3O_4 NPs assembled into flowerlike structures through an aging process, where the surfaces of the PtPb domains fused together with the Fe_3O_4 lobes extending outward. Although the conversion mechanism in this study appears to be selective deposition and reaction with the Pt domain rather than galvanic exchange (due to the nobility of Pt), this study demonstrates the potential for performing such selective reactions.

As a further demonstration of site-selective conversion chemistry, Read *et al* deposited Ag NPs onto the Ge portion of Au-Ge heterodimer NPs through galvanic exchange.[222] The Au-Ge-$(Ag)_n$ NP product featured single domains of Au and Ge and multiple smaller domains of Ag (Fig. 14), which did not undergo alloying with Au.

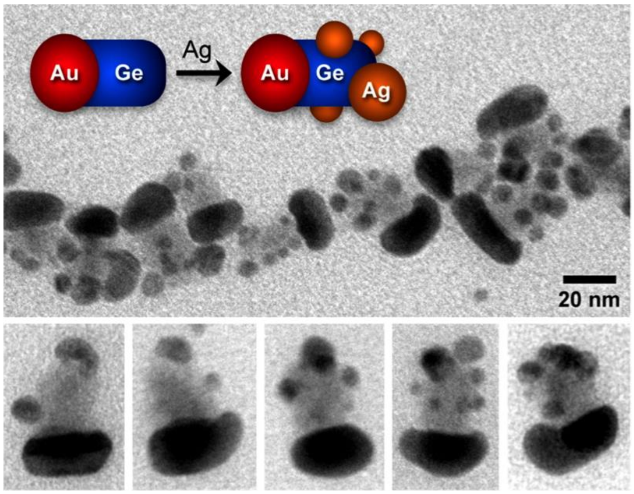

Fig. 14 TEM images of Au-Ge-$(Ag)_n$ NPs. Multiple Ag NPs were deposited onto the Ge domains through a selective galvanic exchange reaction, where the Au domains remained unperturbed. Lower panels display individual heterotrimer NPs. Reprinted with permission from Reference 222. © 2013 American Chemical Society.

10. Concluding Remarks and Vision

NP conversion chemistry is a maturing field, where there are rich opportunities to better understand conversion chemical reaction mechanisms, as well as to explore more complex reactions and materials. Elements or compounds that have not been explored as NP core materials may undergo conversion chemical reactions, and previously unexplored reagents may allow access to new regimes of conversion chemistry. Of the classes of conversion chemical reactions discussed, the least is known about anion exchange, which is usually accompanied by the Kirkendall effect. Studies of how anion exchange drives void formation will give important insights into the mechanism of void formation. Simulations will give a deeper, more detailed understanding of the mechanisms of conversion chemical reactions, and advanced characterization techniques will facilitate atomic-scale understanding. While several examples of controlling the composition, morphology, and crystallinity of the products have been discussed, improved control is still needed in many conversion chemical reactions. Common levers used for controlling conversion chemical reactions include selection of the reactants, concentrations, and the reaction temperature and time. Simultaneously with gaining better understandings and improving control over conversion chemical reactions, there are plentiful opportunities to use NPs synthesized through conversion chemistry in a host of applications.

Three main approaches are anticipated for creating more complex materials through conversion chemistry: (1) use of more complex starting NPs, such as multicomponent NPs, (2) conducting more complex reactions, either using more complex molecular chemistry, or by performing sequential reactions, and (3) combining conversion chemistry with other bottom-up or top-down methods of patterning materials, such as self-assembly or lithography, where the structure will affect the properties of individual NPs and the larger structure.

Some examples of combining assembly or patterning with conversion chemistry already point to the potential of this approach for creating novel materials. In two studies already discussed, self-assembled chains of Au/Co core/shell NPs were converted into chains of Au/Co_3O_4 core/shell NPs,[128] and aligned arrays of Cu nanowires were converted into CuO nanotubes.[132] In another recent study, films of CdSe NPs were converted into films of PbSe, Cu_2Se, or Ag_2Se NPs.[223] Conversion chemical reactions can also be conducted prior to assembly, as demonstrated in a recent study, where triangular Ag nanoplatelets were converted into AuAg, PdAg, or PtAg alloy nanoshells, which were then assembled into hydrogels, followed by supercritical drying.[224] The aerogel products exhibited porosity on two length scales, within the nanoshells, and in the spaces between NPs.

Conversion chemistry gives access to a wide range of metal alloy and metal oxide, sulphide, selenide, and phosphide NPs with complex architectures, including heterostructures, which may be difficult or impossible to obtain using other fabrication techniques. These materials are of interest for a broad range of applications because of their novel catalytic, electronic, optical, magnetic, and electrochemical properties, which enable applications in energy, biomedicine, and sensing.

Applications in energy[225] include electrocatalytic and photocatalytic fuel cells, which utilize the hydrogen evolution reaction (HER),[197] oxygen reduction reaction (ORR),[226–228] and methanol oxidation reaction (MOR).[160,229,230] Hollow NPs obtained through conversion chemistry are also of interest for Li-ion battery technology.[64,231] Multicomponent porous NPs are attractive for applications in catalysis, where the large surface area and alloying noble metals with non-noble metals can both increase catalytic activity and reduce cost.[232,233]

Conversion chemistry is useful for biomedical applications because it can alter the functional properties of materials (such as the surface plasmon resonance of hollow metal nanostructures[159,234–238]) and can also control the shape and porosity of materials, which are also known to affect their behaviour and uptake into biological systems.[239–242] NPs synthesized through conversion chemical reactions have potential for use in cancer therapy,[217] drug delivery,[200,203,210,211,213,243] imaging,[244,245] and biosensing.[246] Recent developments in the conversion chemistry of rare-earth-based NPs (Section 8) make them potentially useful for drug delivery using pores created through anion exchange reactions, while allowing for simultaneous optical and/or magnetic tracking.[247,248]

Gas sensing is another important application of hollow NPs. Controlling the composition and porosity of hollow NPs can enhance their sensing performance. For example, SnO_2 nanotubes doped with Ag_2O NPs obtained through the Kirkendall effect have significantly faster response and recovery times for sensing ethanol and butanone than $Ag/C/SnO_2$ core/shell/shell nanocables.[249] In another study, porous Fe_2O_3 NPs with multiple small voids within each NP had better detection and sensitivity than solid Fe_2O_3 NPs for sensing CO, H_2, NH_3, and vapours from liquefied petroleum gas.[250]

11. Acknowledgements

This work was supported by the National Science Foundation (DMR-1056653).

12. Notes

Department of Materials Science and Engineering, North Carolina State University, Raleigh, NC 27695, USA. E-mail:jbtracy@ncsu.edu

Bryan D. Anderson is a fourth year Ph.D. student in Prof. Tracy's research group in the Department of Materials Science and Engineering at North Carolina State University. After receiving his B.S. in Geology from NC State, he worked as a geologist for Unimin Corporation, where he conducted industrial mineral exploration, and for URS Corporation, where he worked on environmental remediation of contaminated soil and groundwater. In addition to nanoparticle conversion chemistry, his research interests include the synthesis and self-assembly of multifunctional nanoparticles.

Joseph B. Tracy is an Associate Professor in the Department of Materials Science and Engineering at North Carolina State University. He received his B.S. in Chemistry from the University of California, Santa Barbara, and his Ph.D. from MIT in Physical Chemistry, followed by postdoctoral research at the University of North Carolina, Chapel Hill. He joined NC State in 2007, where his research interests include the synthesis, conversion chemistry, self-assembly, and applications of magnetic, metal, and semiconductor nanoparticles. In 2011, he received an NSF CAREER award.

13. References

1. J. Liu, S. Z. Qiao, J. S. Chen, X. W. Lou, X. Xing, and G. Q. Lu, *Chem. Commun.*, 2011, **47**, 12578.
2. Z. Wang, L. Zhou, and X. W. David Lou, *Adv. Mater.*, 2012, **24**, 1903.
3. H. You, S. Yang, B. Ding, and H. Yang, *Chem. Soc. Rev.*, 2013, **42**, 2880.
4. J. Wang, A. C. Johnston-Peck, and J. B. Tracy, *Chem. Mater.*, 2009, **21**, 4462.
5. S. Peng and S. Sun, *Angew. Chem., Int. Ed.*, 2007, **46**, 4155.
6. J. Park, H. Zheng, Y. Jun, and A. P. Alivisatos, *J. Am. Chem. Soc.*, 2009, **131**, 13943.
7. A. Cabot, V. F. Puntes, E. Shevchenko, Y. Yin, L. Balcells, M. a Marcus, S. M. Hughes, and a P. Alivisatos, *J. Am. Chem. Soc.*, 2007, **129**, 10358.
8. Y. Yang, R. Bin Yang, H. J. Fan, R. Scholz, Z. Huang, A. Berger, Y. Qin, M. Knez, and U. Gösele, *Angew. Chem., Int. Ed.*, 2010, **49**, 1442.
9. F. Aldinger, *Acta Metall.*, 1974, **22**, 923.
10. A. Kumar, M. Nasrallah, and D. L. Douglass, *Oxid. Met.*, 1974, **8**, 227.
11. Z. L. Cui, L. F. Dong, and Z. K. Zhang, *Nanostruct. Mater.*, 1995, **5**, 829.
12. D. Potoczna-Petru and L. Krajczyk, *J. Mater. Sci. Lett.*, 1995, **14**, 1294.

13. Y. Yin, R. M. Rioux, C. K. Erdonmez, S. Hughes, G. A. Somorjai, and a P. Alivisatos, *Science*, 2004, **304**, 711.

14. J. Chen, B. Wiley, J. McLellan, Y. Xiong, Z.-Y. Li, and Y. Xia, *Nano Lett.*, 2005, **5**, 2058.

15. X. Gong, Y. Yang, and S. Huang, *J. Phys. Chem. C*, 2010, **114**, 18073.

16. Y. Sun and Y. Xia, *Nano Lett.*, 2003, **3**, 1569.

17. J. Zeng, Q. Zhang, J. Chen, and Y. Xia, *Nano Lett.*, 2010, **10**, 30.

18. L. Au, X. Lu, and Y. Xia, *Adv. Mater.*, 2008, **20**, 2517.

19. J. Chen, J. M. McLellan, A. Siekkinen, Y. Xiong, Z.-Y. Li, and Y. Xia, *J. Am. Chem. Soc.*, 2006, **128**, 14776.

20. M. H. Kim, X. Lu, B. Wiley, E. P. Lee, and Y. Xia, *J. Phys. Chem. C.*, 2008, **112**, 7872.

21. H. Li, M. Zanella, A. Genovese, M. Povia, A. Falqui, C. Giannini, and L. Manna, *Nano Lett.*, 2011, **11**, 4964.

22. U. Jeong, Y. Xia, and Y. Yin, *Chem. Phys. Lett.*, 2005, **416**, 246.

23. P. H. C. Camargo, Y. H. Lee, U. Jeong, Z. Zou, and Y. Xia, *Langmuir*, 2007, **23**, 2985.

24. H. Cheng, B. Huang, X. Qin, X. Zhang, and Y. Dai, *Chem. Commun.*, 2012, **48**, 97.

25. B. J. Beberwyck, Y. Surendranath, and A. P. Alivisatos, *J. Phys. Chem. C*, 2013, **117**, 19759.

26. J. B. Rivest and P. K. Jain, *Chem. Soc. Rev.*, 2013, **42**, 89.

27. W.-S. Wang, L. Zhen, C.-Y. Xu, L. Yang, and W.-Z. Shao, *J. Phys. Chem. C*, 2008, **112**, 19390.

28. S. Chen, X. Zhang, X. Hou, Q. Zhou, and W. Tan, *Cryst. Growth Des.*, 2010, **10**, 1257.

29. S. Mahesh, A. Gopal, R. Thirumalai, and A. Ajayaghosh, *J. Am. Chem. Soc.*, 2012, **134**, 7227.

30. C. L. Kuo and K. C. Hwang, *Chem. Mater.*, 2013, **25**, 365.

31. Y. Sun and Y. Wang, *Nano Lett.*, 2011, **11**, 4386.

32. K. Ding, Z. Miao, B. Hu, G. An, Z. Sun, B. Han, and Z. Liu, *Langmuir*, 2010, **26**, 10294.

33. D.-H. Ha, L. M. Moreau, S. Honrao, R. G. Hennig, and R. D. Robinson, *J. Phys. Chem. C*, 2013, **117**, 14303.

34. Z. Yang, M. Walls, I. Lisiecki, and M. Pileni, *Chem. Mater.*, 2013, **25**, 2372.

35. A. C. Johnston-Peck, J. Wang, and J. B. Tracy, *ACS Nano*, 2009, **3**, 1077.

36. T.-J. Yoon, H. Shao, R. Weissleder, and H. Lee, *Part. Part. Syst. Charact.*, 2013, **30**, 667.

37. A. Brückman, *Corros. Sci.*, 1967, **7**, 51.

38. N. Birks, G. H. Meier, and F. S. Pettit, *Introduction to the High-Temperature Oxidation of Metals*, Cambridge University Press, Cambridge, UK, 2nd edn., 2006.

39. R. Nakamura, J.-G. Lee, D. Tokozakura, H. Mori, and H. Nakajima, *Mater. Lett.*, 2007, **61**, 1060.

40. P. Kofstad, *High-Temperature Oxidation of Metals*, Wiley, New York, 1966.

41. P. Kofstad, *High Temperature Corrosion*, Elsevier Applied Science, London, 1988.

42. M. Schütze, *Protective Oxide Scales and Their Breakdown*, Wiley, Chichester, 1997.

43. J. G. Railsback, A. C. Johnston-Peck, J. Wang, and J. B. Tracy, *ACS Nano*, 2010, **4**, 1913.

44. M. Verelst, T. O. Ely, C. Amiens, E. Snoeck, P. Lecante, A. Mosset, M. Respaud, J. M. Broto, and B. Chaudret, *Chem. Mater.*, 1999, **11**, 2702.

45. X.-C. Sun and X.-L. Dong, *Mater. Res. Bull.*, 2002, **37**, 991.

46. V. Skumryev, S. Stoyanov, Y. Zhang, G. Hadjipanayis, D. Givord, and J. Nogués, *Nature*, 2003, **423**, 850.

47. R. K. Zheng, *J. Appl. Phys.*, 2004, **95**, 5244.

48. K. Sakiyama, K. Koga, T. Seto, M. Hirasawa, and T. Orii, *J. Phys. Chem. B*, 2004, **108**, 523.

49. C. M. Wang, D. R. Baer, L. E. Thomas, J. E. Amonette, J. Antony, Y. Qiang, and G. Duscher, *J. Appl. Phys.*, 2005, **98**, 094308.

50. J. Tracy, D. Weiss, D. Dinega, and M. Bawendi, *Phys. Rev. B*, 2005, **72**, 064404.

51. Y. Yin, C. K. Erdonmez, A. Cabot, S. Hughes, and A. P. Alivisatos, *Adv. Funct. Mater.*, 2006, **16**, 1389.

52. I. S. Lee, N. Lee, J. Park, B. H. Kim, Y.-W. Yi, T. Kim, T. K. Kim, I. H. Lee, S. R. Paik, and T. Hyeon, *J. Am. Chem. Soc.*, 2006, **128**, 10658.

53. R. Nakamura, J.-G. Lee, D. Tokozakura, H. Mori, and H. Nakajima, *Mater. Lett.*, 2007, **61**, 1060.

54. Y. Gao, D. Shindo, Y. Bao, and K. Krishnan, *Appl. Phys. Lett.*, 2007, **90**, 233105.

55. S. Inderhees, J. Borchers, K. Green, M. Kim, K. Sun, G. Strycker, and M. Aronson, *Phys. Rev. Lett.*, 2008, **101**, 117202.

56. K. Yamamoto, S. A. Majetich, M. R. McCartney, M. Sachan, S. Yamamuro, and T. Hirayama, *Appl. Phys. Lett.*, 2008, **93**, 082502.

57. P. A. Chernavskii, G. V. Pankina, V. I. Zaikovskii, N. V. Peskov, and P. Afanasiev, *J. Phys. Chem. C*, 2008, **112**, 9573.

58. X. Zheng, S. Yuan, Z. Tian, S. Yin, J. He, K. Liu, and L. Liu, *Chem. Mater.*, 2009, **21**, 4839.

59. Q. Ong, A. Wei, and X.-M. Lin, *Phys. Rev. B*, 2009, **80**, 134418.

60. L.-I. Hung, C.-K. Tsung, W. Huang, and P. Yang, *Adv. Mater.*, 2010, **22**, 1910.

61. L. Zhang, P. Hu, X. Zhao, R. Tian, R. Zou, and D. Xia, *J. Mater. Chem.*, 2011, **21**, 18279.

62. S. Chenna, R. Banerjee, and P. A. Crozier, *ChemCatChem*, 2011, **3**, 1051.

63. S. Jia, C.-H. Hsia, and D. H. Son, *J. Phys. Chem. C*, 2011, **115**, 92.

64. B. Koo, H. Xiong, M. D. Slater, V. B. Prakapenka, M. Balasubramanian, P. Podsiadlo, C. S. Johnson, T. Rajh, and E. V Shevchenko, *Nano Lett.*, 2012, **12**, 2429.

65. S. Chenna and P. A. Crozier, *Micron*, 2012, **43**, 1188.

66. J. A. Medford, A. C. Johnston-Peck, and J. B. Tracy, *Nanoscale*, 2013, **5**, 155.

67. K.-Y. Niu, J. Park, H. Zheng, and A. P. Alivisatos, *Nano Lett.*, 2013, **13**, 5715.

68. S. Sadasivan, R. M. Bellabarba, and R. P. Tooze, *Nanoscale*, 2013, **5**, 11139.

69. K. Kravchyk, L. Protesescu, M. I. Bodnarchuk, F. Krumeich, M. Yarema, M. Walter, C. Guntlin, and M. V Kovalenko, *J. Am. Chem. Soc.*, 2013, **135**, 4199.

70. N. Cabrera and N. F. Mott, *Rep. Prog. Phys.*, 1949, **12**, 163.

71. V. P. Zhdanov and B. Kasemo, *Chem. Phys. Lett.*, 2008, **452**, 285.

72. A. Ermoline and E. L. Dreizin, *Chem. Phys. Lett.*, 2011, **505**, 47.

73. A. Auge, A. Weddemann, B. Vogel, F. Wittbracht, and A. Hütten, *Appl. Phys. Lett.*, 2010, **96**, 093111.

74. A. Fromhold and E. Cook, *Phys. Rev.*, 1967, **163**, 650.

75. Y. Hwang, S. Angappane, J. Park, K. An, T. Hyeon, and J.-G. Park, *Curr. Appl. Phys.*, 2012, **12**, 808.

76. N. Doan, K. Kontturi, and C. Johans, *J. Colloid Interface Sci.*, 2010, **350**, 126.

77. I. Lisiecki, M. Walls, D. Parker, and M. P. Pileni, *Langmuir*, 2008, **24**, 4295.

78. E. Klecha, D. Ingert, M. Walls, and M. P. Pileni, *Langmuir*, 2009, **25**, 2824.

79. I. Lisiecki, S. Turner, S. Bals, M. P. Pileni, and G. Van Tendeloo, *Chem. Mater.*, 2009, **21**, 2335.

80. E. Klecha, I. Arfaoui, J. Richardi, D. Ingert, and M.-P. Pileni, *Phys. Chem. Chem. Phys.*, 2011, **13**, 2953.

81. Z. Yang, I. Lisiecki, M. Walls, and M.-P. Pileni, *ACS Nano*, 2013, **7**, 1342.

82. W. Wu and M. M. Maye, *Small*, 2014, **10**, 271.

83. R. Nakamura, D. Tokozakura, H. Nakajima, J.-G. Lee, and H. Mori, *J. Appl. Phys.*, 2007, **101**, 074303.

84. S. Jia, C.-H. Hsia, and D. H. Son, *J. Phys. Chem. C*, 2011, **115**, 92.

85. C. Wagner, *Z. Phys. Chem*, 1933, **21**, 25.

86. K. Fueki and J. B. Wagner, *J. Electrochem. Soc.*, 1965, **112**, 384.

87. F. Gesmundo and F. Viani, *Corros. Sci.*, 1978, **18**, 217.

88. G. Valensi, *C. R. Acad. Sci. Paris*, 1936, **202**, 309.

89. G. Valensi, *Compt. Rend*, 1936, **202**, 309.

90. R. E. Carter, *J. Chem. Phys.*, 1961, **35**, 1137.

91. R. E. Carter, *J. Chem. Phys.*, 1961, **34**, 2010.

92. A. Fromhold and E. Cook, *Phys. Rev.*, 1968, **175**, 877.

93. A. T. Fromhold, *J. Phys. Chem. Solids*, 1988, **49**, 1159.

94. L. Zhou, A. Rai, N. Piekiel, X. Ma, and M. R. Zachariah, *J. Phys. Chem. C*, 2008, **112**, 16209.

95. B. J. Henz, T. Hawa, and M. R. Zachariah, *J. Appl. Phys.*, 2010, **107**, 024901.

96. R. Nakamura, D. Tokozakura, J.-G. Lee, H. Mori, and H. Nakajima, *Acta Mater.*, 2008, **56**, 5276.

97. T.-L. Ha, J. G. Kim, S. M. Kim, and I. S. Lee, *J. Am. Chem. Soc.*, 2013, **135**, 1378.

98. R. Nakamura, G. Matsubayashi, H. Tsuchiya, S. Fujimoto, and H. Nakajima, *Acta Mater.*, 2009, **57**, 4261.

99. K. N. Tu and U. Gösele, *Appl. Phys. Lett.*, 2005, **86**, 093111.

100. A. M. Gusak, T. V. Zaporozhets, K. N. Tu, and U. Gösele, *Philos. Mag.*, 2005, **85**, 4445.

101. A. V. Evteev, E. V. Levchenko, I. V. Belova, and G. E. Murch, *Philos. Mag.*, 2007, **87**, 3787.

102. A. V. Evteev, E. V. Levchenko, I. V. Belova, and G. E. Murch, *Philos. Mag.*, 2008, **88**, 1525.

103. R. Nakamura, G. Matsubayashi, H. Tsuchiya, S. Fujimoto, and H. Nakajima, *Acta Mater.*, 2009, **57**, 5046.

104. E. Muthuswamy, P. R. Kharel, G. Lawes, and S. L. Brock, *ACS Nano*, 2009, **3**, 2383.

105. A. E. Henkes, Y. Vasquez, and R. E. Schaak, *J. Am. Chem. Soc.*, 2007, **129**, 1896.

106. A. E. Henkes and R. E. Schaak, *Inorg. Chem.*, 2008, **47**, 671.

107. A. Earnshaw and N. Greenwood, *Chemistry of the Elements*, Elsevier Butterworth-Heinemann, Oxford, 2nd edn., 1997.

108. R.-K. Chiang and R.-T. Chiang, *Inorg. Chem.*, 2007, **46**, 369.

109. A. E. Henkes and R. E. Schaak, *Chem. Mater.*, 2007, **19**, 4234.

110. E. Muthuswamy, G. H. L. Savithra, and S. L. Brock, *ACS Nano*, 2011, **5**, 2402.

111. E. Muthuswamy and S. L. Brock, *Chem. Commun.*, 2011, **47**, 12334.

112. S. Carenco, Y. Hu, I. Florea, O. Ersen, C. Boissière, N. Mézailles, and C. Sanchez, *Chem. Mater.*, 2012, **24**, 4134.

113. D. P. Dinega and M. G. Bawendi, *Angew. Chem., Int. Ed.*, 1999, **38**, 1788.

114. S. Sun and C. B. Murray, *J. Appl. Phys.*, 1999, **85**, 4325.

115. D.-H. Ha, L. M. Moreau, C. R. Bealing, H. Zhang, R. G. Hennig, and R. D. Robinson, *J. Mater. Chem.*, 2011, **21**, 11498.

116. Z. Wang, L. Pan, H. Hu, and S. Zhao, *CrystEngComm*, 2010, **12**, 1899.

117. S. Gullapalli, J. M. Grider, H. G. Bagaria, K.-S. Lee, M. Cho, V. L. Colvin, G. E. Jabbour, and M. S. Wong, *Nanotechnology*, 2012, **23**, 495605.

118. G. Xiao, Y. Zeng, Y. Jiang, J. Ning, W. Zheng, B. Liu, X. Chen, G. Zou, and B. Zou, *Small*, 2013, **9**, 793.

119. M. Ibáñez, J. Fan, W. Li, D. Cadavid, R. Nafria, A. Carrete, and A. Cabot, *Chem. Mater.*, 2011, **23**, 3095.

120. H. J. Fan, M. Knez, R. Scholz, D. Hesse, K. Nielsch, M. Zacharias, and U. Gösele, *Nano Lett.*, 2007, **7**, 993.

121. X. Liang, X. Wang, Y. Zhuang, B. Xu, S. Kuang, and Y. Li, *J. Am. Chem. Soc.*, 2008, **130**, 2736.

122. A. Cabot, R. K. Smith, Y. Yin, H. Zheng, B. M. Reinhard, H. Liu, and A. P. Alivisatos, *ACS Nano*, 2008, **2**, 1452.

123. M. F. Sarac, W.-C. Wu, and J. B. Tracy, *Chem. Mater.*, 2014, **26**, 3057.

124. Z. Nie, A. Petukhova, and E. Kumacheva, *Nat. Nanotechnol.*, 2010, **5**, 15.

125. L. J. Hill and J. Pyun, *ACS Appl. Mater. Interfaces*, 2014, **6**, 6022.

126. J. B. Tracy and T. M. Crawford, *MRS Bull.*, 2013, **38**, 915.

127. B. Y. Kim, I.-B. Shim, Z. O. Araci, S. S. Saavedra, O. L. a Monti, N. R. Armstrong, R. Sahoo, D. N. Srivastava, and J. Pyun, *J. Am. Chem. Soc.*, 2010, **132**, 3234.

128. B. Y. Kim, S.-H. Yu, H. S. Kim, D.-C. Lee, I.-B. Shim, S. E. Derosa, Y.-E. Sung, and J. Pyun, *J. Mater. Chem.*, 2011, **21**, 14163.

129. P. Y. Keng, M. M. Bull, I. Shim, K. G. Nebesny, N. R. Armstrong, Y. Sung, K. Char, and J. Pyun, *Chem. Mater.*, 2011, **23**, 1120.

130. L. De Trizio, A. Figuerola, L. Manna, A. Genovese, C. George, R. Brescia, Z. Saghi, R. Simonutti, M. Van Huis, and A. Falqui, *ACS Nano*, 2012, **6**, 32.

131. Y. Ren, W. K. Chim, S. Y. Chiam, J. Q. Huang, C. Pi, and J. S. Pan, *Adv. Funct. Mater.*, 2010, **20**, 3336.

132. A.-A. El Mel, M. Buffière, P.-Y. Tessier, S. Konstantinidis, W. Xu, K. Du, I. Wathuthanthri, C.-H. Choi, C. Bittencourt, and R. Snyders, *Small*, 2013, **9**, 2838.

133. S. Jeong, M. T. McDowell, and Y. Cui, *ACS Nano*, 2011, **5**, 5800.

134. H. Sun, Y. Chen, X. Wang, Y. Xie, W. Li, and X. Zhang, *J. Nanopart. Res.*, 2011, **13**, 97.

135. S.-B. Wang, W. Zhu, J. Ke, J. Gu, A.-X. Yin, Y.-W. Zhang, and C.-H. Yan, *Chem. Commun.*, 2013, **49**, 7168.

136. C. E. Carlton, S. Chen, P. J. Ferreira, L. F. Allard, and Y. Shao-Horn, *J. Phys. Chem. Lett.*, 2012, **3**, 161.

137. L. Dubau, F. Maillard, M. Chatenet, J. André, and E. Rossinot, *Electrochim. Acta*, 2010, **56**, 776.

138. L. Dubau, J. Durst, F. Maillard, L. Guétaz, M. Chatenet, J. André, and E. Rossinot, *Electrochim. Acta*, 2011, **56**, 10658.

139. C. Chen, Y. Kang, Z. Huo, Z. Zhu, W. Huang, H. L. Xin, J. D. Snyder, D. Li, J. A. Herron, M. Mavrikakis, M. Chi, K. L. More, Y. Li, N. M. Markovic, G. A. Somorjai, P. Yang, and V. R. Stamenkovic, *Science*, 2014, **343**, 1339.

140. J. Erlebacher and D. Margetis, *Phys. Rev. Lett.*, 2014, **112**, 155505.

141. M. Lopez-Haro, L. Dubau, L. Guétaz, P. Bayle-Guillemaud, M. Chatenet, J. André, N. Caqué, E. Rossinot, and F. Maillard, *Appl. Catal., B*, 2014, **152-153**, 300.

142. S. Jana, J. W. Chang, and R. M. Rioux, *Nano Lett.*, 2013, **13**, 3618.

143. E. A. Anumol, C. Nethravathi, and N. Ravishankar, *Part. Part. Syst. Charact.*, 2013, **30**, 590.

144. X. Xia, Y. Wang, A. Ruditskiy, and Y. Xia, *Adv. Mater.*, 2013, **25**, 6313.

145. Y. Sun and Y. Xia, *Nano Lett.*, 2003, **3**, 1569.

146. Q. Zhang, J. Xie, J. Y. Lee, J. Zhang, and C. Boothroyd, *Small*, 2008, **4**, 1067.

147. V. Bansal, H. Jani, J. Du Plessis, P. J. Coloe, and S. K. Bhargava, *Adv. Mater.*, 2008, **20**, 717.

148. M. Mohl, A. Kumar, A. L. M. Reddy, A. Kukovecz, Z. Konya, I. Kiricsi, R. Vajtai, and P. M. Ajayan, *J. Phys. Chem. C*, 2010, **114**, 389.

149. I. Najdovski, A. P. O'Mullane, and S. K. Bhargava, *Electrochem. Commun.*, 2010, **12**, 1535.

150. Q. Cui, Y. Sha, J. Chen, and Z. Gu, *J. Nanopart. Res.*, 2011, **13**, 4785.

151. M. Clay, Q. Cui, Y. Sha, J. Chen, A. J. Rondinone, Z. Wu, J. Chen, and Z. Gu, *Mater. Lett.*, 2012, **88**, 143.

152. Y. Sun, B. Wiley, Z.-Y. Li, and Y. Xia, *J. Am. Chem. Soc.*, 2004, **126**, 9399.

153. X. Lu, L. Au, J. McLellan, Z.-Y. Li, M. Marquez, and Y. Xia, *Nano Lett.*, 2007, **7**, 1764.

154. X. Teng, Q. Wang, P. Liu, W. Han, A. I. Frenkel, W. Wen, N. Marinkovic, J. C. Hanson, and J. A. Rodriguez, *J. Am. Chem. Soc.*, 2008, **130**, 1093.

155. M. H. Kim, X. Lu, B. Wiley, E. P. Lee, and Y. Xia, *J. Phys. Chem. C.*, 2008, **112**, 7872.

156. J. Zeng, Q. Zhang, J. Chen, and Y. Xia, *Nano Lett.*, 2010, **10**, 30.

157. M. Mohl, D. Dobo, A. Kukovecz, Z. Konya, K. Kordas, J. Wei, R. Vajtai, and P. M. Ajayan, *J. Phys. Chem. C*, 2011, **115**, 9403.

158. Y. Ridelman, G. Singh, R. Popovitz-Biro, S. G. Wolf, S. Das, and R. Klajn, *Small*, 2012, **8**, 654.

159. D. Wan, X. Xia, Y. Wang, and Y. Xia, *Small*, 2013, **9**, 3111.

160. W. Zhang, J. Yang, and X. Lu, *ACS Nano*, 2012, **6**, 7397.

161. E. González, J. Arbiol, and V. F. Puntes, *Science*, 2011, **334**, 1377.

162. Y.-H. Chien, M.-F. Tsai, V. Shanmugam, K. Sardar, C.-L. Huang, and C.-S. Yeh, *Nanoscale*, 2013, **5**, 3863.

163. K. A. Kozek, K. M. Kozek, W.-C. Wu, S. R. Mishra, and J. B. Tracy, *Chem. Mater.*, 2013, **25**, 4537.

164. M. Pradhan, J. Chowdhury, S. Sarkar, A. K. Sinha, and T. Pal, *J. Phys. Chem. C*, 2012, **116**, 24301.

165. G. McNay, D. Eustace, W. E. Smith, K. Faulds, and D. Graham, *Appl. Spectrosc.*, 2011, **65**, 825.

166. Karvianto and G. M. Chow, *J. Nanopart. Res.*, 2012, **14**, 1186.

167. L. Polavarapu and L. M. Liz-Marzán, *Nanoscale*, 2013, **5**, 4355.

168. C. Wang, S. Peng, R. Chan, and S. Sun, *Small*, 2009, **5**, 567.

169. M. S. Shore, J. Wang, A. C. Johnston-Peck, A. L. Oldenburg, and J. B. Tracy, *Small*, 2011, **7**, 230.

170. Y. Sun, B. T. Mayers, and Y. Xia, *Nano Lett.*, 2002, **2**, 481.

171. Y. Yin, C. Erdonmez, S. Aloni, and A. P. Alivisatos, *J. Am. Chem. Soc.*, 2006, **128**, 12671.

172. X. Lu, H.-Y. Tuan, J. Chen, Z.-Y. Li, B. A. Korgel, and Y. Xia, *J. Am. Chem. Soc.*, 2007, **129**, 1733.

173. K.-Y. Niu, S. A. Kulinich, J. Yang, A. L. Zhu, and X.-W. Du, *Chem. Eur. J.*, 2012, **18**, 4234.

174. M. Jin, H. Zhang, J. Wang, X. Zhong, N. Lu, Z. Li, Z. Xie, M. J. Kim, and Y. Xia, *ACS Nano*, 2012, **6**, 2566.

175. S. Xie, M. Jin, J. Tao, Y. Wang, Z. Xie, Y. Zhu, and Y. Xia, *Chem. Eur. J.*, 2012, **18**, 14974.

176. M. Jin, G. He, H. Zhang, J. Zeng, Z. Xie, and Y. Xia, *Angew. Chem., Int. Ed.*, 2011, **50**, 10560.

177. H.-P. Liang, L.-J. Wan, C.-L. Bai, and L. Jiang, *J. Phys. Chem. B*, 2005, **109**, 7795.

178. A. M. Schwartzberg, T. Y. Olson, C. E. Talley, and J. Z. Zhang, *J. Phys. Chem. B*, 2006, **110**, 19935.

179. M. Chen and L. Gao, *Inorg. Chem.*, 2006, **45**, 5145.

180. M. Mohl, A. Kumar, A. L. M. Reddy, A. Kukovecz, Z. Konya, I. Kiricsi, R. Vajtai, and P. M. Ajayan, *J. Phys. Chem. C*, 2010, **114**, 389.

181. M. H. Oh, T. Yu, S.-H. Yu, B. Lim, K.-T. Ko, M.-G. Willinger, D.-H. Seo, B. H. Kim, M. G. Cho, J.-H. Park, K. Kang, Y.-E. Sung, N. Pinna, and T. Hyeon, *Science*, 2013, **340**, 964.

182. M. Saruyama, Y.-G. So, K. Kimoto, S. Taguchi, Y. Kanemitsu, and T. Teranishi, *J. Am. Chem. Soc.*, 2011, **133**, 17598.

183. B. J. Beberwyck and A. P. Alivisatos, *J. Am. Chem. Soc.*, 2012, **134**, 19977.

184. D. H. Son, S. M. Hughes, Y. Yin, and A. Paul Alivisatos, *Science*, 2004, **306**, 1009.

185. Y. Feldman, E. Wasserman, D. J. Srolovitz, and R. Tenne, *Science*, 1995, **267**, 222.

186. Y. Feldman, G. L. Frey, M. Homyonfer, V. Lyakhovitskaya, L. Margulis, H. Cohen, G. Hodes, J. L. Hutchison, and R. Tenne, *J. Am. Chem. Soc.*, 1996, **118**, 5362.

187. E. Muthuswamy and S. L. Brock, *J. Am. Chem. Soc.*, 2010, **132**, 15849.

188. S. Xiong and H. C. Zeng, *Angew. Chem., Int. Ed.*, 2012, **51**, 949.

189. J. Gopalakrishnan, S. Pandey, and K. K. Rangan, *Chem. Mater.*, 1997, **9**, 2113.

190. X. Huang, M. Wang, M. Willinger, L. Shao, D. S. Su, and X. Meng, *ACS Nano*, 2012, **6**, 7333.

191. H. Zhang, L. V Solomon, D.-H. Ha, S. Honrao, R. G. Hennig, and R. D. Robinson, *Dalt. Trans.*, 2013, **42**, 12596.

192. P. Cai, D.-K. Ma, Q.-C. Liu, S.-M. Zhou, W. Chen, and S.-M. Huang, *J. Mater. Chem. A*, 2013, **1**, 5217.

193. I. T. Sines, D. D. Vaughn, A. J. Biacchi, C. E. Kingsley, E. J. Popczun, and R. E. Schaak, *Chem. Mater.*, 2012, **24**, 3088.

194. X. Xia, C. Zhu, J. Luo, Z. Zeng, C. Guan, C. F. Ng, H. Zhang, and H. J. Fan, *Small*, 2013, **10**, 766.

195. Z. Wu, B. Fang, A. Bonakdarpour, A. Sun, D. P. Wilkinson, and D. Wang, *Appl. Catal., B*, 2012, **125**, 59.

196. Z. Zang, H.-B. Yao, Y. Zhou, W. Yao, and S. Yu, *Chem. Mater.*, 2008, **20**, 4749.

197. Y. Xu, R. Wu, J. Zhang, Y. Shi, and B. Zhang, *Chem. Commun.*, 2013, **49**, 6656.

198. I. T. Sines and R. E. Schaak, *J. Am. Chem. Soc.*, 2011, **133**, 1294.

199. S. Zhuo, Y. Xu, W. Zhao, J. Zhang, and B. Zhang, *Angew. Chem., Int. Ed.*, 2013, **52**, 8602.

200. Z. Xu, P. Ma, C. Li, Z. Hou, X. Zhai, S. Huang, and J. Lin, *Biomaterials*, 2011, **32**, 4161.

201. G. Tian, Z. Gu, X. Liu, L. Zhou, W. Yin, L. Yan, S. Jin, W. Ren, G. Xing, S. Li, and Y. Zhao, *J. Phys. Chem. C*, 2011, **115**, 23790.

202. T. Grzyb, A. Gruszeczka, R. J. Wiglusz, Z. Śniadecki, B. Idzikowski, and S. Lis, *J. Mater. Chem.*, 2012, **22**, 22989.

203. X. Kang, D. Yang, P. Ma, Y. Dai, M. Shang, D. Geng, Z. Cheng, and J. Lin, *Langmuir*, 2013, **29**, 1286.

204. L. Zhang, H. Jiu, Y. Fu, Y. Sun, P. Chen, Y. Li, and S. Ma, *Mater. Lett.*, 2013, **101**, 47.

205. Y. Gao, M. Fan, Q. Fang, and W. Han, *New J. Chem.*, 2013, **37**, 670.

206. X. Kang, D. Yang, Y. Dai, M. Shang, Z. Cheng, X. Zhang, H. Lian, P. Ma, and J. Lin, *Nanoscale*, 2013, **5**, 253.

207. J. Zhang, Y. Wang, L. Guo, and P. Dong, *Dalton Trans.*, 2013, **42**, 3542.

208. D. Chen, L. Lei, J. Xu, A. Yang, and Y. Wang, *Nanotechnology*, 2013, **24**, 085708.

209. F. Zhang, Y. Shi, X. Sun, D. Zhao, and G. D. Stucky, *Chem. Mater.*, 2009, **21**, 5237.

210. R. Lv, S. Gai, Y. Dai, F. He, N. Niu, and P. Yang, *Inorg. Chem.*, 2014, **53**, 998.

211. R. Lv, S. Gai, Y. Dai, N. Niu, F. He, and P. Yang, *ACS Appl. Mater. Interfaces*, 2013, **5**, 10806.

212. L. Zhang, M. Yin, H. You, M. Yang, Y. Song, and Y. Huang, *Inorg. Chem.*, 2011, **50**, 10608.

213. Z. Xu, Y. Cao, C. Li, P. Ma, X. Zhai, S. Huang, X. Kang, M. Shang, D. Yang, Y. Dai, and J. Lin, *J. Mater. Chem.*, 2011, **21**, 3686.

214. J. Zhang, Y. Wang, Z. Xu, H. Zhang, P. Dong, L. Guo, F. Li, S. Xin, and W. Zeng, *J. Mater. Chem. B*, 2013, **1**, 330.

215. T. Teranishi and M. Sakamoto, *J. Phys. Chem. Lett.*, 2013, **4**, 2867.

216. E. V. Shevchenko, M. I. Bodnarchuk, M. V. Kovalenko, D. V. Talapin, R. K. Smith, S. Aloni, W. Heiss, and A. P. Alivisatos, *Adv. Mater.*, 2008, **20**, 4323.

217. J. Gao, G. Liang, B. Zhang, Y. Kuang, X. Zhang, and B. Xu, *J. Am. Chem. Soc.*, 2007, **129**, 1428.

218. R. E. Schaak and M. E. Williams, *ACS Nano*, 2012, **6**, 8492.

219. M. R. Buck, J. F. Bondi, and R. E. Schaak, *Nat. Chem.*, 2012, **4**, 37.

220. L. J. Hill, M. M. Bull, Y. Sung, A. G. Simmonds, P. T. Dirlam, N. E. Richey, S. E. DeRosa, I.-B. Shim, D. Guin, P. J. Costanzo, N. Pinna, M.-G. Willinger, W. Vogel, K. Char, and J. Pyun, *ACS Nano*, 2012, **6**, 8632.

221. M. J. Bradley, A. J. Biacchi, and R. E. Schaak, *Chem. Mater.*, 2013, **25**, 1886.

222. C. G. Read, A. J. Biacchi, and R. E. Schaak, *Chem. Mater.*, 2013, **25**, 4304.

223. J. B. Rivest, R. Buonsanti, T. E. Pick, L. Zhu, E. Lim, C. Clavero, E. Schaible, B. A. Helms, and D. J. Milliron, *J. Am. Chem. Soc.*, 2013, **135**, 7446.

224. K. G. S. Ranmohotti, X. Gao, and I. U. Arachchige, *Chem. Mater.*, 2013, **25**, 3528.

225. M. Fayette and R. D. Robinson, *J. Mater. Chem. A*, 2014, **2**, 5965.

226. S. J. Bae, S. J. Yoo, Y. Lim, S. Kim, Y. Lim, J. Choi, K. S. Nahm, S. J. Hwang, T.-H. Lim, S.-K. Kim, and P. Kim, *J. Mater. Chem.*, 2012, **22**, 8820.

227. Y. Zhang, C. Ma, Y. Zhu, R. Si, Y. Cai, J. X. Wang, and R. R. Adzic, *Catal. Today*, 2013, **202**, 50.

228. H.-H. Li, C.-H. Cui, S. Zhao, H.-B. Yao, M.-R. Gao, F.-J. Fan, and S.-H. Yu, *Adv. Energy Mater.*, 2012, **2**, 1182.

229. B. Y. Xia, H. Bin Wu, X. Wang, and X. W. Lou, *J. Am. Chem. Soc.*, 2012, **134**, 13934.

230. X. Huang, Y. Chen, E. Zhu, Y. Xu, X. Duan, and Y. Huang, *J. Mater. Chem. A*, 2013, **1**, 14449.

231. Y. Hu, X. Huang, K. Wang, J. Liu, J. Jiang, R. Ding, X. Ji, and X. Li, *J. Solid State Chem.*, 2010, **183**, 662.

232. D. A. Cantane, F. E. R. Oliveira, S. F. Santos, and F. H. B. Lima, *Appl. Catal., B*, 2013, **136-137**, 351.

233. L. Dubau, J. Durst, F. Maillard, L. Guétaz, M. Chatenet, J. André, and E. Rossinot, *Electrochim. Acta*, 2011, **56**, 10658.

234. S. E. Skrabalak, J. Chen, L. Au, X. Lu, X. Li, and Y. Xia, *Adv. Mater.*, 2007, **19**, 3177.

235. S. E. Skrabalak, J. Chen, Y. Sun, X. Lu, L. Au, C. M. Cobley, and Y. Xia, *Acc. Chem. Res.*, 2008, **41**, 1587.

236. Y. Xia, W. Li, C. M. Cobley, J. Chen, X. Xia, Q. Zhang, M. Yang, E. C. Cho, and P. K. Brown, *Acc. Chem. Res.*, 2011, **44**, 914.

237. W. Li, P. K. Brown, L. V Wang, and Y. Xia, *Contrast Media Mol. Imaging*, 2011, **6**, 370.

238. G. D. Moon, S.-W. Choi, X. Cai, W. Li, E. C. Cho, U. Jeong, L. V Wang, and Y. Xia, *J. Am. Chem. Soc.*, 2011, **133**, 4762.

239. J. E. Gagner, M. D. Lopez, J. S. Dordick, and R. W. Siegel, *Biomaterials*, 2011, **32**, 7241.

240. S. Dasgupta, T. Auth, and G. Gompper, *Nano Lett.*, 2014, **14**, 687.

241. R. Agarwal, V. Singh, P. Jurney, L. Shi, S. V Sreenivasan, and K. Roy, *Proc. Natl. Acad. Sci. U. S. A.*, 2013, **110**, 17247.

242. S. Barua, J.-W. Yoo, P. Kolhar, A. Wakankar, Y. R. Gokarn, and S. Mitragotri, *Proc. Natl. Acad. Sci. U. S. A.*, 2013, **110**, 3270.

243. K. Cheng, S. Peng, C. Xu, and S. Sun, *J. Am. Chem. Soc.*, 2009, **131**, 10637.

244. J. Gao, G. Liang, J. S. Cheung, Y. Pan, Y. Kuang, F. Zhao, B. Zhang, X. Zhang, E. X. Wu, and B. Xu, *J. Am. Chem. Soc.*, 2008, **130**, 11828.

245. C. Wang, Y. Wang, L. Xu, X. Shi, X. Li, X. Xu, H. Sun, B. Yang, and Q. Lin, *Small*, 2013, **9**, 413.

246. H. Zhu, J. Wang, and G. Xu, *Cryst. Growth Des.*, 2009, **9**, 633.

247. C. Bouzigues, T. Gacoin, and A. Alexandrou, *ACS Nano*, 2011, **5**, 8488.

248. S. Gai, C. Li, P. Yang, and J. Lin, *Chem. Rev.*, 2014, **114**, 2343.

249. X. Chen, Z. Guo, W.-H. Xu, H.-B. Yao, M.-Q. Li, J.-H. Liu, X.-J. Huang, and S.-H. Yu, *Adv. Funct. Mater.*, 2011, **21**, 2049.

250. N. D. Cuong, T. T. Hoa, D. Q. Khieu, N. D. Hoa, and N. Van Hieu, *Curr. Appl. Phys.*, 2012, **12**, 1355.

Table of Contents Entry

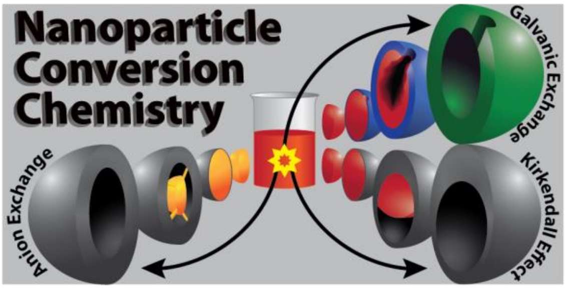

Review article discussing recent advances in conversion chemistry of nanoparticles through the Kirkendall effect, galvanic exchange, and anion exchange.

Cover Graphic